energy&fuels

pubs.acs.org/EF Review

Overview of Asphaltene Nanostructures and Thermodynamic Applications

Bruno Schuler, Yunlong Zhang, Fang Liu, Andrew E. Pomerantz, A. Ballard Andrews, Leo Gross, Vincent Pauchard, Sanjoy Banerjee, and Oliver C. Mullins*

Cite This: https://dx.doi.org/10.1021/acs.energyfuels.0c00874 Read Online

ACCESS | Metrics & More | Article Recommendations

ABSTRACT: Previously, asphaltene science had been hindered by many significant uncertainties regarding molecular weight, molecular structure, and nanocolloidal characteristics in laboratory solvents and crude oils. These debates were of sufficient magnitude to forestall development and utility of asphaltene modeling for various applications. In the last 2 decades, advances in asphaltene science using many sophisticated techniques have greatly reduced corresponding uncertainties, enabling development of simple asphaltene models for a variety of applications. Here, we provide an overview of key findings in asphaltene science; dominant molecular and nanocolloidal structures are described. These structures with simple thermodynamic formalisms are shown to work well in oilfield reservoirs, specifically including light oils, black oils, and heavy oils. This novel thermodynamic approach using asphaltene nanostructures has enabled characterization of different processes that impact or preclude equilibration of reservoir fluids in geologic time. These processes combine to form the new technical discipline, "reservoir fluid geodynamics", that has proven value in many reservoir studies. In addition, these asphaltene nanostructures are shown to apply to interfacial tension of asphaltene solutions, using simple thermodynamics for surfaces. In addition, we contrast past and current debates in asphaltene science, especially regarding asphaltene molecular architecture, which has been largely resolved. Molecular structural characterization of asphaltenes reviewed herein shows that asphaltenes are dominated by island structures, but some asphaltenes also have a secondary content of structures with an "aryl-linked core", which we propose as a third class of molecular architecture along with island and archipelago designations. The aryl-linked core structure is defined as having a single, contiguous sp^2-hybridized carbon network containing one or more aryl linkages, in which adjacent aromatic rings are directly bonded together but do not share a common bond in a ring. In contrast, a traditional island structure also has a single, contiguous sp^2-hybridized carbon network but has adjacent aromatic rings exclusively fused (sharing a common bond in a ring) with no aryl linkages. The definition of archipelago remains unchanged and consists of multiple, discontinuous sp^2-hybridized carbon networks, in which these different aromatic ring systems are connected by one or more sp^3-hybridized carbons. This new classification, "aryl-linked core", has been assigned to both island and archipelago structures in different publications; thus, this new designation should reduce confusion and help resolve structure−function relations, especially regarding aggregation and reactivity. More broadly, the advances in asphaltene science have ushered in powerful, new applications that are continuing to expand.

INTRODUCTION

Asphaltene science has been subject to many debates regarding a variety of issues.[1−4] In the past, some of these debates were of such magnitude and significance that advances in the field were thwarted; these issues had to be resolved. The most important had been the order of magnitude (or more) uncertainties regarding asphaltene molecular weight.[1,5−13] Naturally, with such a large uncertainty in molecular weight, asphaltene molecular architecture was also unknown. These fundamental uncertainties in asphaltene science had precluded adherence to Francis Crick's axiom "to understand function, study structure".

Many if not most of the major uncertainties regarding asphaltenes have largely been resolved, and several of these advances are codified in the Yen−Mullins model shown in Figure 1.[14,15] A large number of experimental and modeling results have been incorporated into this model. The most pernicious, prior uncertainty about asphaltenes had been the ≥10× uncertainty in molecular weight. A specific complexity of asphaltenes is that they exhibit hierarchical nanocolloidal aggregation in both laboratory solvents and reservoir crude oils.[14−17] That is, asphaltenes have three thresholds of solubility in contrast to most solute−solvent systems that exhibit only a single solubility threshold. At low concentrations, asphaltenes are dispersed as a true molecular solution. At higher concentrations, asphaltenes are dispersed as nanoaggregates. At yet higher concentrations, asphaltenes are dispersed as clusters of nanoaggregates. With a further

Special Issue: In Honor of Professor Michael Klein

Received: March 19, 2020
Revised: May 4, 2020
Published: May 6, 2020

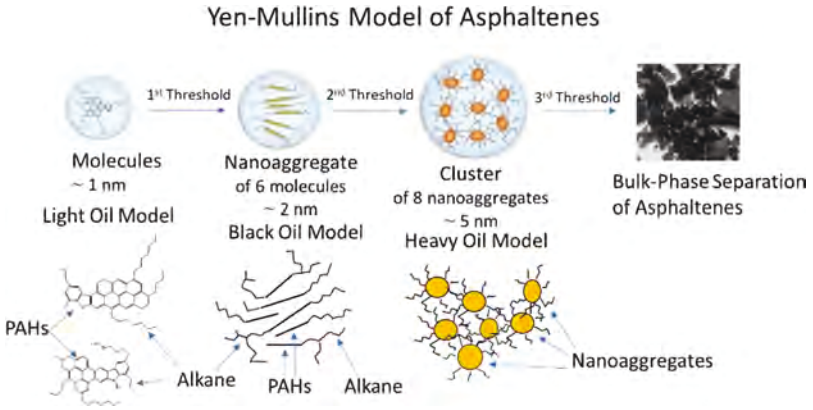

Figure 1. Yen–Mullins model showing typical structures for molecules, nanoaggregates, and clusters.[14,15] Asphaltenes exhibit three solubility thresholds in laboratory solvents and reservoir crude oils. Thermodynamic modeling, such as for asphaltene gradients in oilfield reservoirs, requires such centroid structures.[16−18] Prior to its resolution, this complex, hierarchical nanocolloidal structure exacerbated early debates in asphaltene science.

concentration increase, asphaltenes undergo bulk phase separation.

YEN–MULLINS MODEL

A very brief summary is provided of many of the key measurements that went into development of the Yen–Mullins model in Figure 1.[14,15] There is now broad agreement for the molecular weight of asphaltenes obtained from both molecular diffusion measurements and mass spectrometry. Molecular diffusion measurements included time-resolved fluorescence depolarization (TRFD),[5,6,19−21] Taylor dispersion,[22] fluorescence correlation spectroscopy,[23−25] and nuclear magnetic resonance (NMR).[26−30] Mass spectrometry methods included electrospray ionization, Fourier transform ion cyclotron resonance mass spectrometry (ESI–FT-ICR–MS),[7,8,31−33] laser desorption ionization mass spectrometry (LDI MS),[9,10,34] laser-induced acoustic desorption mass spectrometry (LIAD MS),[35] tandem mass spectrometry,[36,37] atmospheric pressure chemical ionization mass spectrometry (APCI MS),[38] and laser desorption, laser ionization mass spectrometry (L^2MS).[12,13,39−42] The proposed dominance of a single polycyclic aromatic hydrocarbon (PAH) core for asphaltenes arose from TRFD measurements[5,6,19−21] and is consistent with small molecular weights and relatively large-asphaltene PAHs known from optical interrogation.[43−46] TRFD measurements are sensitive only to fluorescent molecules, prompting some concern that non-fluorescent asphaltene molecules may have a different structure. Subsequently, the proposed island structure was strongly supported by the L^2MS unimolecular decomposition technique, which was demonstrated to be comparably sensitive to nearly all components of asphaltenes.[41,42] In addition, this island molecular architecture is consistent with other mass spectrometry measurements.[36] Recently, direct single-molecule imaging by atomic force microscopy (AFM) and scanning tunneling microscopy (STM) provided exact structures of many asphaltene molecules.[47,48] Analysis of 10 very diverse asphaltenes confirms the dominance of island molecules, that is molecules with a single PAH core in all cases. A secondary contributing structure in some samples has a single core containing all aromatic carbon of the molecule but with different aromatic moieties connected by one or more aryl linkages; this class was definitively established in these imaging experiments for the first time.[47,48] Molecular architecture is addressed in greater detail in subsequent sections of this paper.

Nanoaggregate formation (of ∼6 or 7 molecules) is a fundamental property of asphaltenes of all kinds.[14,15,49,50] Nanoaggregates can remain stably suspended in reservoir crude oils for geologic time; these are stable and not metastable species.[17,51,52] The critical nanoaggregate concentration (CNAC) has been determined by many methods relying on different physics, such as high-Q ultrasonics,[53,54] direct current (DC) conductivity,[55−57] NMR,[26−30] centrifugation of both asphaltene–toluene solutions[57,58] and live crude oils.[59] The aggregation number (∼6 or 7 molecules per nanoaggregate) has been shown precisely by surface-assisted laser desorption/ionization mass spectrometry (SALDI MS),[40,49,60] and roughly other methods, including by analysis of gravity gradients of asphaltenes in oilfield reservoirs.[17,51,52] The structure of nanoaggregates with an interior of a PAH stack and an exterior of alkane carbon (cf. Figure 1) has been shown by combined studies of small-angle neutron scattering (SANS) and small-angle X-ray scattering (SAXS).[61−63] Molecular modeling is consistent with this result.[50]

Clusters represent the second aggregation phase.[14,15] Similar to nanoaggregates, clusters (of ∼8 nanoaggregates) can remain stably suspended in crude oil for geologic time.[17,64,65] There is no evidence of a third hierarchical aggregate species that remains stable for geologic time.[17] The fact that unstable asphaltene colloidal particles have been measured to be as small as 10 nm supports this perspective.[66,67] The critical clustering concentration (CCC) has been measured by the kinetics of floc formation[68,69] and combined DC conductivity and centrifugation studies.[57] The approximate aggregation number of clusters (∼8 nanoaggregates) has been determined by several methods, including combined SANS and SAXS studies[61−63] as well as gravitational gradient studies of asphaltenes in heavy oil columns over enormous length scales.[64]

Asphaltenes are defined by their solubility characteristics being bulk-phase-unstable in *n*-heptane and soluble (or nanocolloidally suspended) in toluene. Bulk phase separation of asphaltenes can occur from either the addition of too much solute, the asphaltenes, or a reduction of solvency of the solvent. Both processes are well-known in oilfield reservoirs. An increase of solution gas causes a reduction of asphaltene solvency and frequently causes bulk phase separation of heavy

https://dx.doi.org/10.1021/acs.energyfuels.0c00874
Energy Fuels XXXX, XXX, XXX–XXX

ends, which are generally referred to as asphaltenes in the oilfield but may also include other components in addition to asphaltenes.[17,70−72] The addition of asphaltenes to a solution or crude oil can easily cause the solvency capacity to be exceeded, whether laboratory solvent or crude oil. If the asphaltenes are added in the form of 5 nm clusters, then the solution can become supersaturated and bulk phase separation proceeds. This process is also known in oilfield reservoirs.[17,64,73]

FLORY−HUGGINS−ZUO EQUATION OF STATE (FHZ EOS)

Each of the three representations for the three different species (molecules, nanoaggregates, and clusters) in Figure 1 is meant to represent the centroid of the distribution. Knowledge of the centroid might be sufficient for some applications. That is, despite the enormous variety of asphaltene molecular structures, certain physical properties can be described as if the compound would consist of a single "effective" structure only. This "effective" molecule, aggregate, or cluster is guided by the Yen−Mullins model. For example, for the modeling of gravitational gradients of asphaltenes in oil reservoirs through measurements of the optical density, the centroid of the specific molecular species in Figure 1 is sufficient.[16,17,51,52,64,74,75] Nevertheless, the great variety of different asphaltene molecules is emphasized below.

The FHZ EoS is perhaps the simplest, realistic approach to model asphaltene gradients. The FHZ EoS includes a gravity term, which requires the size of the asphaltene species from Figure 1. The FHZ EoS also has a single chemical interaction parameter each for the solute and solvent, the Hildebrand solubility parameter. Within a given oil column, this parameter is essentially constant for asphaltenes and depends primarily upon gas−oil ratio (GOR) for the crude oil.[76] Indeed, the asphaltene solubility parameter is fixed almost universally, including for petroleum asphaltenes, coal-derived asphaltenes, and immature source rock bitumen asphaltenes.[76] It is reasonable that these asphaltenes, which are constrained to have the same solubility characteristics, all have the same solubility parameter. The FHZ model is shown below in eq 1.[16,18,77]

$$\frac{\mathrm{OD}_\lambda(h_2)}{\mathrm{OD}_\lambda(h_1)} = \frac{\varphi_a(h_2)}{\varphi_a(h_1)} = \exp\left\{\frac{v_a g(\rho - \rho_a)(h_2 - h_1)}{RT} + \frac{v_a}{RT}[(\delta_a - \delta)^2_{h_1} - (\delta_a - \delta)^2_{h_2}] + \left[\left(\frac{v_a}{v}\right)_{h_2} - \left(\frac{v_a}{v}\right)_{h_1}\right]\right\} \quad (1)$$

where $\mathrm{OD}_\lambda(h_i)$ is the optical density of the crude oil at wavelength λ at height h_i in the reservoir, R is the universal gas constant, $\varphi_a(h_i)$ is the volume fraction of asphaltene in the crude oil at height h_i in the reservoir, v is the molar volume of oil, v_a is the molar volume of asphaltene, δ is the Hildebrand solubility parameter of the oil, δ_a is the Hildebrand solubility parameter of the asphaltenes, T is the temperature, g is the gravitational acceleration, ρ is the oil density, and ρ_a is the asphaltene density. The solubility parameter, molar volume, and density of bulk fluids, temperature, pressure, and compositions are dependent upon depth. As written, both δ and δ_a are considered to be a function of height h_i in the oil column, thus, the subscript h_i on the difference term. In practice, δ_a is invariant for a given reservoir oil, and only δ is a function of height. The primary effect of height on δ is via GOR gradients. Methane has a lower solubility parameter than other oil components, and higher GOR oils are also lower density. Both factors cause a polarizability dependence δ upon GOR gradients. The FHZ EoS is a mathematical relation between the pressure, volume, temperature, and compositions. The concentration (volume fraction) variations of asphaltenes with depth depend upon three terms in order in eq 1: gravity, solubility (enthalpy), and entropy.

APPLICATION OF THE FHZ EOS WITH THE YEN−MULLINS MODEL

Figure 2 shows the application of the FHZ EoS with a molecular dispersion of asphaltenes in a light oil from a North Sea reservoir.[17,75] Figure 2A shows an image of the oilfield with its fluids, where green is oil, dark red is gas, and blue is water. This oil has a low asphaltene content of less than 0.5%, consistent with a molecular dispersion of asphaltenes. The asphaltene content (as determined by oil color from downhole measurements[78]) versus height or true vertical depth subsea (TVDss) in the oil column is plotted in Figure 2B for various heights in the oil column for six wells in the field. Two outliers are observed, a lighter oil and a heavier oil; the physical barriers in the reservoir that isolate these oils are known.[75,79] Their differing asphaltene content occurs because these oils are different maturities and, being isolated, could not equilibrate with the crude oil in the main body of the reservoir.[79]

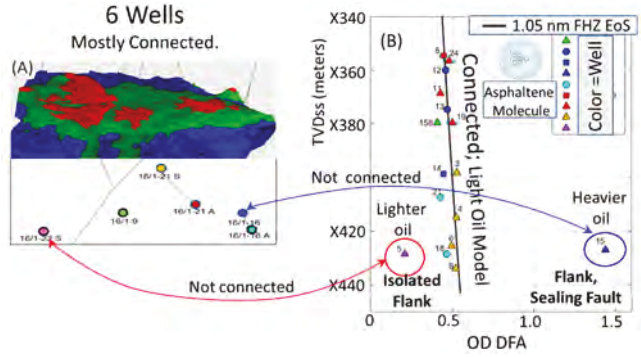

Figure 2. Asphaltene gradient in this light oil reservoir (Norway) matches the FHZ EoS presuming the molecular size in the Yen−Mullins model (1.05 nm diameter for an equivalent sphere).[17,75] The relative asphaltene content is determined downhole by the optical density (OD), here at 815 nm wavelength.[78] Equilibrium modeling with the use of the FHZ EoS is consistent with reservoir connectivity in terms of fluid flow, which is known from oil production.[79] The lighter oil (red circle) and heavier oil (blue circle) are isolated from the oils in the main body of the reservoir by known geologic features. These two oils differ in maturity (not shown);[79] the low asphaltene content oil is high maturity, while the high asphaltene content oil is low maturity.[80] TVDss is true vertical depth subsea. The leading "X" in the depths conceals the absolute depth, which is proprietary.

The gradient in Figure 2 is very small (little change of OD with height) corresponding to the small size of the molecules. In addition, there is very little gradient of GOR of the oil (little change of GOR with height); the crude oils flashed in geologic time in the reservoir as a result of its fairly low pressure, causing the formation of gas caps from this flashed gas. Consequently, the GOR and its gradient are both low. This crude oil is readily modeled with the FHZ EoS and its reliance

https://dx.doi.org/10.1021/acs.energyfuels.0c00874
Energy Fuels XXXX, XXX, XXX−XXX

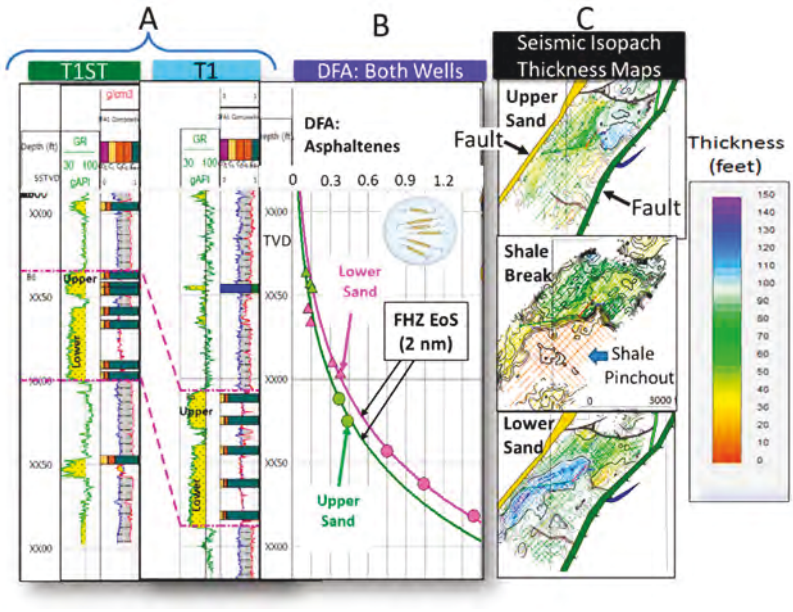

Figure 3. Black oil reservoir.[17,81] (A) Upper sand and lower sand are shown for two wells, T1ST and T1. (B) Downhole fluid analysis (DFA) data for each sand shows that the asphaltene gradient matches the FHZ EoS for 2 nm nanoaggregates. This indicates that each sand is well-connected, as known from production.[81] The offset of the asphaltene gradient curves from each other shows that the upper and lower sands are not well-connected to each other. (C) Isopach thickness maps show that the upper sand is quite thick and that the lower sand is also quite thick, which is consistent with each sand being well-connected. The isopach map of the intervening shale between the sands shows that it is substantial throughout much of the reservoir, thereby limiting connectivity of the upper to lower sands, as gleaned from the offset of the asphaltene gradient curves.[17,81] TVDss is true vertical depth subsea. The leading "XX" in the depths conceals the absolute depth, which is proprietary.

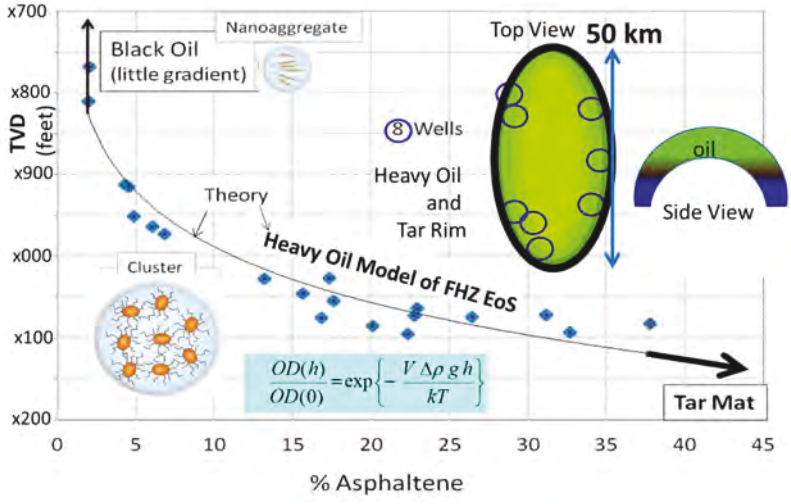

Figure 4. Asphaltene gradients in the heavy oil rim of an anticlinal oil field. Insets show the top view and side view of this anticline.[17,64,73] The asphaltenes exhibit a factor of 10 variation in concentration in the heavy oil rim over a height of 200 ft and over a distance of 100 km. This huge gradient is readily modeled with the FHZ EoS using asphaltene clusters, with no adjustable variables.[17,64,73] TVDss is true vertical depth subsea. The leading "x" in the depths conceals the absolute depth, which is proprietary.

on the molecules of the Yen−Mullins model. No width to the distribution is needed for this purpose, just the typical molecule.[17,75]

Figure 3 shows the application of the FHZ for a black oil reservoir in deep water, Gulf of Mexico.[17,81] This oil has several percent asphaltene, which is consistent with a nanoaggregate dispersion of asphaltenes. The FHZ EoS analyses of the oils in the upper sand and separately in the lower sand indicate thermodynamic equilibration of the oils in each sand, thereby suggesting connectivity of fluid flow within each sand. Such connectivity is known from production.[81] The larger asphaltene gradient in the black oil reservoir compared to the light oil reservoir in Figure 2 is due in part to the larger size of the nanoaggregate versus the molecule. In addition, this black oil has a significant GOR gradient, which drives a solubility gradient and contributes to the asphaltene gradient. This crude oil is readily modeled with the FHZ EoS coupled with the nanoaggregate of the Yen−Mullins model. No width to the distribution is needed for this purpose, just the typical nanoaggregate.[17,81]

Figure 4 shows the application of the FHZ EoS to heavy oil. Because the GOR is very low for this heavy oil, the FHZ EoS

https://dx.doi.org/10.1021/acs.energyfuels.0c00874
Energy Fuels XXXX, XXX, XXX−XXX

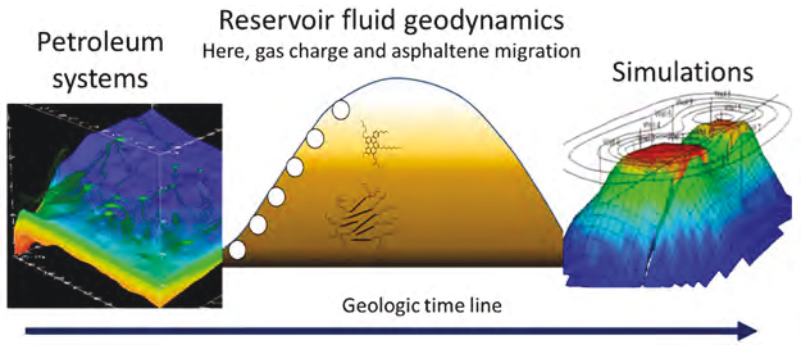

Figure 5. RFG.[17] Asphaltene thermodynamic evaluation of reservoir fluids by the FHZ EoS and its reliance on the Yen−Mullins model has enabled elucidation of the extent of equilibration of reservoir fluids and, thus, fluid processes in geologic time that preclude equilibrium.[17,82,86,87] This capability resolves a long-standing deficiency in the characterization of oilfield reservoirs. RFG falls between petroleum system analysis and reservoir simulations on a geologic timeline.[17,82,86,87]

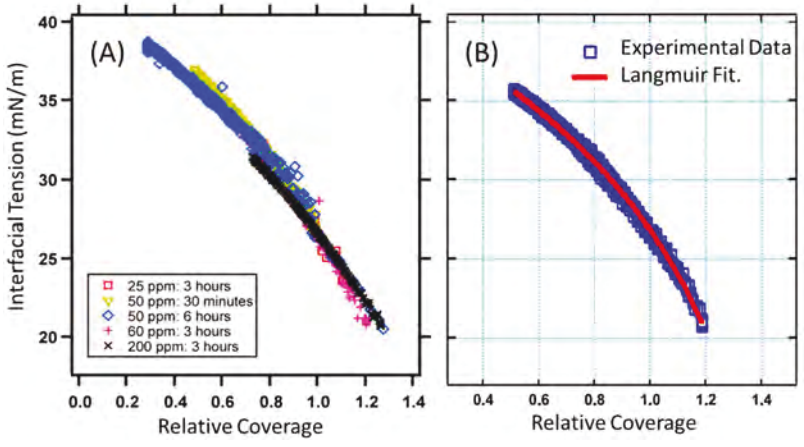

Figure 6. IFT between an asphaltene solution and water.[29] (A) Universal curve is obtained at low to moderate concentrations for all conditions, including variable concentrations and aging times. (B) Langmuir EoS accounts for the asphaltene IFT curve with a minimum number of parameters.

essentially reduces to the gravity term, which is simply Archimedes buoyancy in the Boltzmann distribution (highlighted in blue in Figure 4). The data from seven wells (one well depicted did not penetrate this reservoir) over the 100 km perimeter of the field matches the FHZ EoS using 5.1 nm asphaltene clusters. This compares very favorably to the nominal 5 nm asphaltene clusters published years before this oilfield case study.[17,64,73] This crude oil is readily modeled with the FHZ EoS and its reliance on the clusters of the Yen−Mullins model. No width to the distribution is needed for this purpose, just the typical cluster.[17,64,73]

RESERVOIR FLUID GEODYNAMICS (RFG)

The development of asphaltene thermodynamics in the FHZ EoS with its reliance on the Yen−Mullins model has enabled the routine ability to identify equilibration of reservoir fluids by observation and analysis of asphaltene gradients vertically and laterally in reservoirs.[17,51,52,64,75,82] In many reservoir case studies, it is evident that determination of solution gas equilibrium by cubic EoS analysis is not sufficient to launch the new discipline RFG. In general, the error bars for the GOR measurement are too large, the gradients are too small, and for flashed reservoirs, often there is minimal GOR difference, even in separate compartments.[17] The ability to identify equilibrium of reservoir fluids means that disequilibrium of reservoir fluids can also be identified.[17,70,74,82−84] When disequilibrium is observed, it is generally the case that one or more fluid processes occurring in geologic time can be identified that preclude equilibrium. The collection of these fluid processes defines RFG.[17,82] This discipline is founded in thermodynamic analysis to elucidate time dependence in geologic time and complements geochemical analysis of reservoir fluids (Figure 5).[17,85]

RFG has proven to be of great value to address all manners of reservoir complexities in ∼50 oilfield RFG studies to date. Key issues that have been addressed include reservoir connectivity[51,52] and its inverse compartmentalization,[88,89] baffling,[83,90] viscous oil and tar mat formation,[64,83] upstructure mobile tar,[91] aquifer support,[81] asphaltene onset pressure,[92,93] wax precipitation, solution gas gradients,[84] timing of charge,[94] fault block migration,[95,96] biogenic gas charge into oil,[65] and spill−fill trap filling,[85,97] along with traditional geochemical concerns of biodegradation,[79,85,98] gas washing,[65] and water washing.[85,97,99] These wide-ranging concerns treated in various RFG oilfield studies establish that the development and application of asphaltene thermodynamics extends far beyond issues that are directly impacted by asphaltenes, such as tar mat formation. Instead, RFG exploits thermodynamics, which itself is unlimited in its applications.[17,82,87,100−105]

https://dx.doi.org/10.1021/acs.energyfuels.0c00874
Energy Fuels XXXX, XXX, XXX−XXX

ASPHALTENE INTERFACIAL TENSION

In addition to modeling bulk solution properties, interfacial properties of asphaltene solutions can also be modeled using simple equations along with the centroid of asphaltene molecular properties.[28−30] The specific molecular properties can be compared to that in Figure 1 of the Yen−Mullins model.

The Langmuir equation of state (EoS) accounts for the effect of asphaltenes on the interfacial tension (IFT) and is given below

$$\gamma(\Gamma) = \gamma_o + kT\Gamma_\infty \ln(1 - \Gamma/\Gamma_\infty) \quad (2)$$

where $\gamma(\Gamma)$ is the interfacial tension, γ_o is the clean surface interfacial tension, Γ is the surface coverage, Γ_∞ is the maximum surface coverage, k is the Boltzmann constant, and T is the temperature. The Langmuir EoS is perhaps the simplest equation that can be used to fit IFT data, as shown in Figure 6. There are two adjustable parameters, a reference surface coverage (Γ) and the size of the molecular footprint of the surfactant on the surface (Γ_∞).

The fit to the IFT data in Figure 6 yields a value of the asphaltene molecular footprint equal to a nominal six-ring PAH, which applies to the universal curve shown in Figure 6A. The corresponding characteristic PAH size is remarkably close to the molecular structure shown in Figure 1 in the Yen−Mullins model.[29] This analysis and interpretation require that the asphaltene PAH is in-plane at the oil−water interface and that the alkanes are out-of-plane. Exactly this configuration has been measured for asphaltenes in Langmuir−Blodgett films by sum frequency generation (SFG).[106] These studies also show that PAHs with peripheral oxygen functions orient such that the PAHs were transverse to the interface.[106] These results are consistent with the finding that asphaltene intermolecular interactions are dominated by polarizability of the PAH in solution studies.[107] Alkylated hexabenzocoronene is also oriented with the PAH in-plane at the oil−water interface.[30]

Figure 6 shows that the interfacial tension measurements for many experimental conditions reduce to a universal curve that is fit by the Langmuir equation.[28−30] The excellent fit of the Langmuir equation with its minimum number of parameters to the universal curve lends validity to this analysis. In addition, the concentrations used to obtain the universal curve included values below and above the critical nanoaggregate concentration (CNAC); in these experiments, the CNAC was determined by NMR. This indicates that the nanoaggregates are not surface-active in this concentration range; the surfactant contact area at the interface in the Langmuir equation analysis remained molecular and was unaffected by the presence of nanoaggregates in the bulk solution. Otherwise, IFT data from concentrations in excess of the CNAC would diverge from the universal curve. The nanoaggregate has peripheral alkanes, as shown in Figure 1 and as measured by combined SAXS and SANS experiments.[61−63] The different attraction to the interface of the asphaltene PAH versus alkane is shown in the SFG experiments[106] and is also obtained in coarse-grained modeling.[108] Consequently, the interfacial tension of asphaltene solutions with water is consistent with the Langmuir equation coupled with the Yen−Mullins model over a wide range of experimental conditions.

TIME DEPENDENCE OF ASPHALTENE IFT

An oft-repeated observation of asphaltene IFT is best explained by incorporating more than just the centroid of the asphaltene molecular distribution.[109] Figure 6 shows that the bulk of asphaltene IFT can be accounted for by relative coverage of the surface, independent of surface aging times. However, a more detailed examination of the asphaltene IFT versus aging time shows that there is a small yet readily measurable continuous decline. This is in contrast to the adsorption behavior of a standard single-component surfactant.

Figure 7 plots the IFT data for asphaltene solutions and shows that there is a large drop of IFT at short times and that

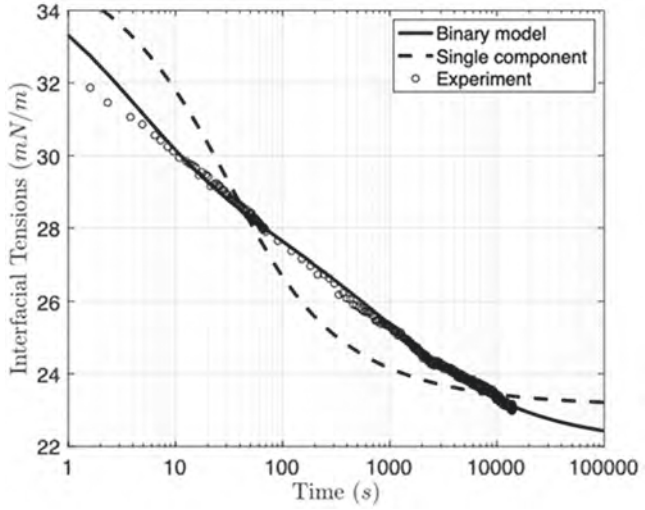

Figure 7. IFT of asphaltene solutions versus time: experiment[110] and modeling.[109] Most of the change occurs at short times. Nevertheless, at long times, the IFT continues to decline. A model with a single surfactant predicts a stable value of the IFT at long times. Models that include two (or more) types of asphaltene molecules can account for the continuous decline of the IFT at long times.[109,110]

the IFT continues to decline at long times.[110] These data are consistent with other studies of the IFT between water and toluene−asphaltene solutions.[111] At short times, diffusion delivers the surfactant to the interface. For a single surfactant, as time progresses, the surface becomes saturated with the surfactant and the IFT ceases to change. Figure 7 shows that the IFT between water and asphaltene solutions continues to decline at long times.[110] A "binary" model that fits the data consists of two types of asphaltene surfactants: one surfactant is present at a higher concentration and accounts for most of the decline of IFT at short times,[109] and a second component with higher interfacial activity and lower concentration eventually diffuses to the interface and replaces some of the original surfactant there. This binary model accounts for the measured data. More components would obviously improve the fitting but at the expense of more parameters.

The analytical solution for this diffusion-controlled adsorption model with a linear isotherm has been worked out as[112]

$$\Pi = \Delta\gamma_{eq}\left[1 - \exp\left(\frac{\tau}{\tau_D}\right)\mathrm{erfc}\left(\sqrt{\frac{\tau}{\tau_D}}\right)\right] \quad (3)$$

where Π is the surface pressure, the reduction of surface tension at equilibrium $\Delta\gamma_{eq} = RTK_HC_b$, with R is the gas

https://dx.doi.org/10.1021/acs.energyfuels.0c00874
Energy Fuels XXXX, XXX, XXX−XXX

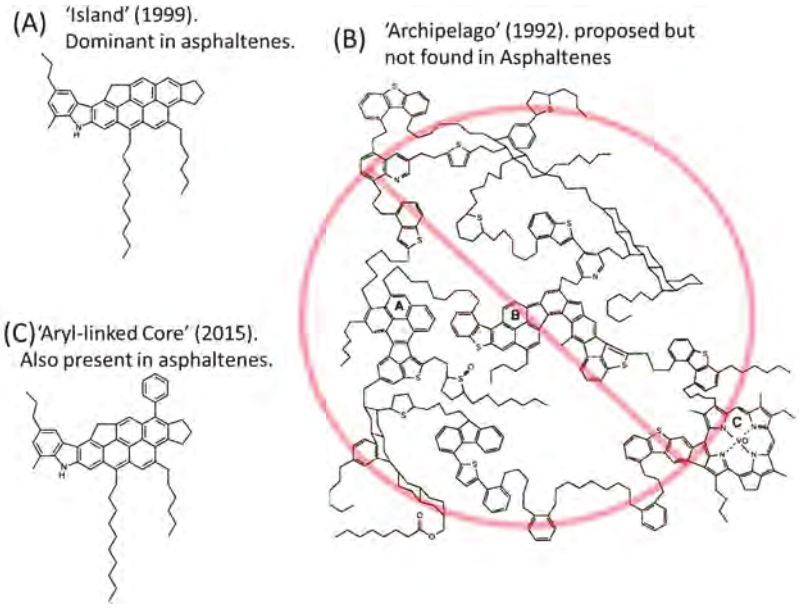

Figure 8. Asphaltene molecular characterization has changed over time. (A) Dominant asphaltene molecular structure.[5,6,41,47,48] (B) In the early 1990s, the widely accepted view was that of the archipelago model.[115,117] TRFD experiments in late 1999 indicated that asphaltenes consist of relatively small molecules with predominantly a single PAH, the island model.[5,6,19−21,120] The debate of island versus archipelago model was represented by panel A versus panel B. Today, there is little debate that the molecular weight represented in panel A is correct. The current debate of island versus archipelago has reduced largely to that between panels A and C. To reflect this vastly improved situation and to avoid confusion with previous debilitating debates (inhibiting advancement), the authors propose to introduce a third type of asphaltene molecular label, "aryl-linked core", for asphaltene molecules that possess a core with all aromatic carbon of the molecule and with one or more aryl linkage between aromatic moieties; this class of structures was first definitively shown by AFM imaging.[47,48]

constant, T is the temperature, K_H is Henry's law constant, and C_b is the bulk concentration, τ is the time, and the characteristic diffusion time $\tau_D = K_H^2/D$, with D is the diffusion constant.

In the mixture case of Langmuir-type adsorption, the surface excess coverage Γ_∞ is assumed to be (almost) the same for all of the components and the fractional surface coverage θ_i of the ith component becomes[109]

$$\theta_i = \frac{k_i C_{si}}{1 + \sum k_j C_{sj}} \tag{4}$$

where k_i is the adsorption constant of component i (the ratio of the adsorption rate constant over the desorption rate constant) and C_{si} is the subsurface concentration of component i. The binary model employed in Figure 7 uses two species with different interfacial activities. Nevertheless, both species are presumed to have the same molecular contact area at the interface.[109] This is consistent with the data presented in Figure 6. The component of a higher surface activity would give rise to a slightly higher ultimate surface coverage. At high coverage, only a small change of surface coverage is needed to cause a significant change of IFT.[113] In contrast, at a low surface coverage, a very large change of surface coverage is needed to cause a change of IFT.[113] In addition, this treatment helps keep the number of adjustable parameters to a minimum. This assumption is also consistent with the measurement of different surfactant species in asphaltenes.[114] If a third component of even higher interfacial activity and even lower concentration is present in asphaltenes, then the predicted reduction of surface tension with time would occur for very long times.

As with bulk phase distributions of asphaltenes, modeling the IFT sometimes can proceed with consideration only of the centroid of the molecular distribution. For other applications, greater complexity of the distribution of the molecular or colloidal components of asphaltenes must be considered. A minimum number of parameters help reveal the proper chemistry and physics of the system, as opposed to providing merely curve fitting of data. With a sufficiently large number of parameters, many models can fit experimental data, whether the underlying fundamental physics is correct or not.

■ ASPHALTENE MOLECULAR CHARACTERIZATION AND ITS CHANGE OVER TIME

Figure 1 provides the overview of asphaltene molecules that is consistent with a broad array of results. However, asphaltene molecular weight and, thus, molecular architecture were subjects of extensive debate in the field. In particular, prior to the understanding of the complex hierarchical aggregation of asphaltenes shown in Figure 1, many studies were negatively impacted by unrecognized asphaltene aggregation. In particular, aggregate properties were often ascribed to molecular properties.[11]

Vapor pressure osmometry (VPO) studies were performed on asphaltenes to determine molecular weight. VPO requires fairly high solute concentrations, and in VPO studies on asphaltenes, the lowest concentrations were comparable to or below that of cluster formation but not the formerly unrecognized nanoaggregate formation.[11] VPO has been used successfully on other crude oil components; therefore, naturally, VPO was extended to asphaltenes. Consequently, very high "molecular" weights were obtained, and corresponding molecular models were generated with covalent linkage of many chemical moieties, the so-called archipelago model shown in Figure 8B.[115] That is, these large molecular weights required cross-linking different chemical moieties, including

https://dx.doi.org/10.1021/acs.energyfuels.0c00874
Energy Fuels XXXX, XXX, XXX−XXX

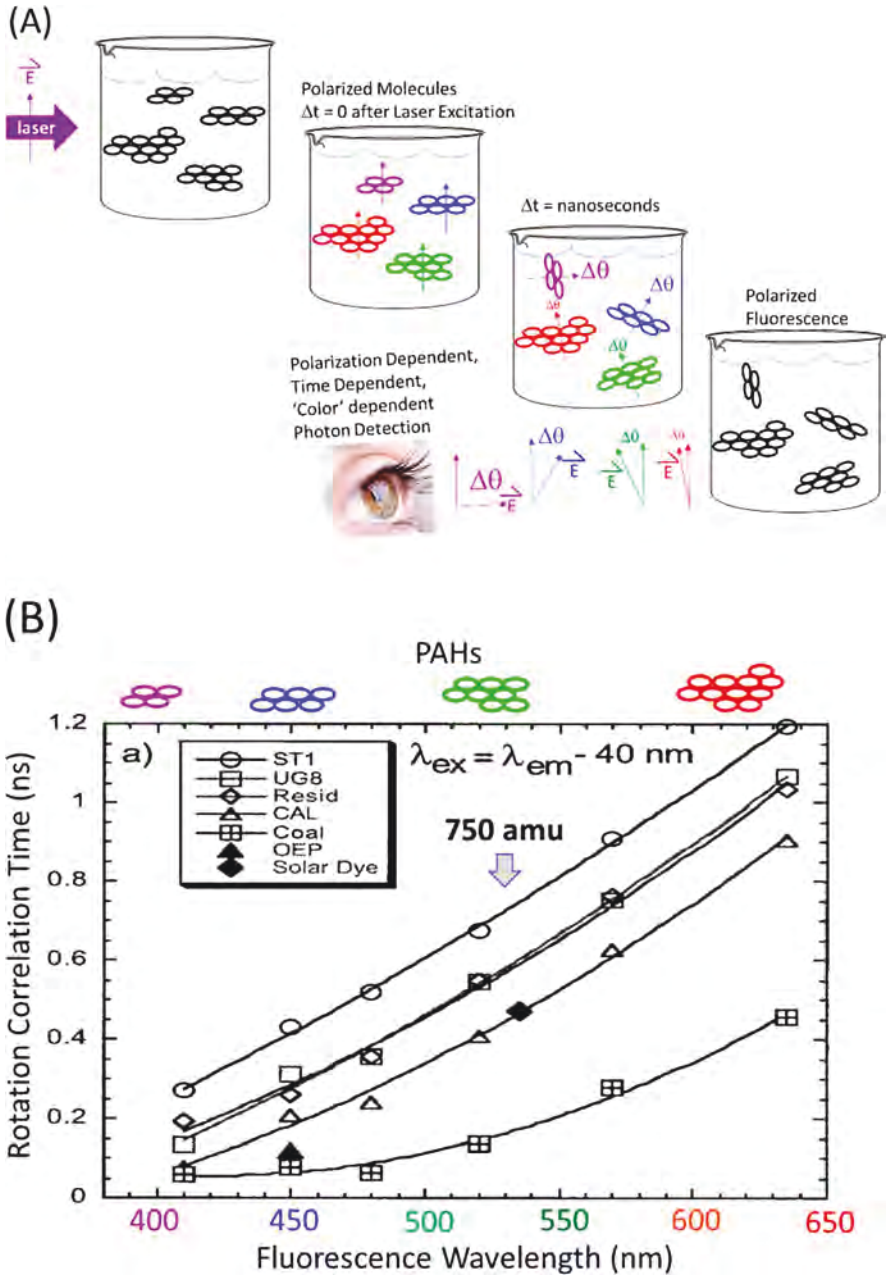

Figure 9. TRFD asphaltenes.[6] (A) Schematic showing the faster rotational diffusion of molecules with a single, small, blue fluorophore and the slower rotational diffusion of molecules with a single, large, red fluorophore. (B) TRFD data for many asphaltenes shows that asphaltenes are small molecules with large diffusion constants comparable to a 750 amu model compound. In addition, asphaltenes have predominantly a single fluorophore (or PAH).[5,6] Cross-linked fluorophores as in Figure 9B would not be characterized by a factor of 10 difference in rotational diffusion times of small and large PAHs.

different PAHs, into a single molecule. LDI MS had been used on asphaltene, but this method is also susceptible to asphaltene aggregation[9,10] and also gave inaccurate and large asphaltene molecular weights. There were early mass spectral results that gave much smaller molecular weights for asphaltenes;[116] however, the twin problems of possible molecular fragmentation and possible inability to volatilize the heavier fraction of asphaltene molecules both gave rise to concerns of inaccurate molecular weights that were deemed too small. The type of molecule shown in Figure 8B was widely viewed as representative of asphaltenes in the 1990s.[115,117] For example, heavy end pyrolysis results had long been interpreted as supporting the existence of archipelago structures, such as in Figure 8B.[118] However, in pyrolysis, archipelago molecules can be synthesized from island structures;[119] thus, studying structure by studying function, the inverse of Crick's axiom, can be problematic.

The first molecular diffusion measurements of asphaltenes gave very different conclusions from the contemporaneous consensus view that asphaltenes were dominated by high molecular weights and archipelago molecular structures. TRFD measurements of asphaltenes obtained large diffusion constants, indicating that asphaltene molecules are relatively small (~750 amu).[5,6,19−21] In addition, these studies showed that the small, blue fluorescing PAHs of asphaltenes were found to undergo rotational diffusion 10 times faster than the larger red

https://dx.doi.org/10.1021/acs.energyfuels.0c00874
Energy Fuels XXXX, XXX, XXX−XXX

fluorescing PAHs. This indicates that these different PAHs are not cross-linked; thus, there is predominantly one PAH per molecule.[5,6,19−21] This is the origin of the so-called island molecular model of asphaltenes, as shown in Figure 8A, and thus the debate of island versus archipelago (Figure 8B) in asphaltenes. Figure 9A shows a schematic of TRFD, and Figure 9B shows the corresponding TRFD data for many asphaltenes.

The twin results of large diffusion constants and a single PAH per molecule from the TRFD studies are internally consistent.[5,6,19−21] Likewise, the ∼10× larger molecular weights that had been obtained by VPO are consistent with the archipelago model with many cross-linked chemical moieties, as indicated in Figure 8B. Over time, many different methods showed that asphaltenes in fact have lower molecular weights, and the corresponding molecular weight debate faded away. Nevertheless, determination of the asphaltene molecular structure remained less certain, and this uncertainty continued to be framed as island versus archipelago, even though the number of proposed cross-linked PAHs of proposed archipelago structures was reduced to accommodate smaller molecular weights. Currently, a structure with only two cross-linked PAHs is called archipelago in stark contrast to the original terminology. In particular, TRFD and mass spectrometry results, such as from L^{2}MS, presented immediately below agreed that the most probable weight was around 700 or 750 amu.

Asphaltenes are 50:50 aromatic/aliphatic carbon (from non-controversial ^{13}C NMR measurements),[21,121,122] which means 350 amu of aromatics. In addition, the asphaltenes have large electronic absorption in the near ultraviolet (UV) and visible range.[43−45,123] That is, the asphaltenes are dark brown, and the color is due to the PAHs.[43−45,123] Moreover, this color cannot be washed out of asphaltenes; the color is intrinsic.[43−45,123] To reproduce the optical absorption profile of asphaltenes, large ring systems (∼7 rings and larger) must be prominent.[45] Accounting for the molecular weight and the color limits the number of PAHs per molecule to one or at most two for the majority of the sample.

The fact that TRFD methods gave molecular weights that were in agreement with many subsequent mass spectral results lends credence to the molecular architecture results from TRFD. These results were important to establish small molecular weights and island architecture as main contributors to asphaltenes. However, TRFD cross sections are not at all uniform for different asphaltene structures. Fluorescence is required for TRFD, and fluorescence cross sections vary widely.[124] Flat cross sections for all asphaltene molecular types are very important to validate average properties.

MOLECULAR WEIGHT BY L^{2}MS

For any mass spectrometric method, asphaltene molecules must be liberated into the vacuum (or vapor). In LDI MS, a single laser is used to both desorb and ionize the asphaltenes simultaneously. It has been demonstrated that this can lead to singly charged ions of aggregates as opposed to molecules, thereby yielding artificially high "molecular" weights.[9,10] The aggregation problem in LDI MS is worse with increased density of the volatilized plume, which results from both higher laser power and higher mass density of asphaltenes on the desorption sample holder.[9,10] Other methods of mass spectrometry have shown the potential impact of asphaltene aggregates.[33]

To avoid aggregation, the functions of desorption and ionization can each be accomplished with separate lasers; this is the basis of L^{2}MS.[12,13,41,42,125−127] An infrared (IR) laser is used to rapidly heat and desorb neutral asphaltene molecules. At some later time, a second laser, typically UV, can be used to ionize the gas-phase asphaltene molecules, which are then mass-analyzed by time of flight. The plume of neutrals has less propensity to aggregate than ions. By the time the asphaltenes are ionized by the second laser, they are dispersed in the vacuum and no longer collide; therefore, aggregates cannot form. With independent controls on desorption and ionization, aggregation can demonstrably be avoided.

The rapid heating of 10^8 K/s afforded by the IR laser is known to suppress fragmentation as well as aggregation.[128] L^{2}MS studies of strongly aggregating compounds, such as caffeic acid, establish this capability.[126] It is also evident in the inset in Figure 10 that all of the asphaltene sample is volatilized

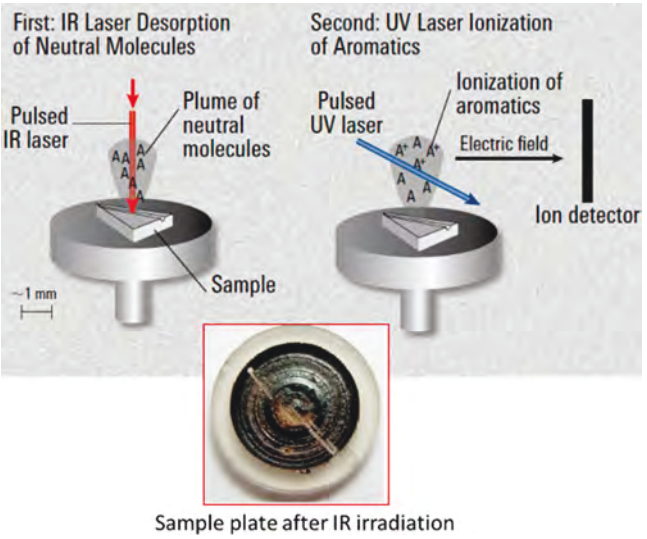

Figure 10. Schematic depicting L^{2}MS.[12,40] The first laser pulse, the IR laser, desorbs the asphaltene sample into the vacuum as a neutral plume. The UV laser pulse ionizes some of the molecules that are then mass-analyzed by time of flight. L^{2}MS suppresses aggregation and fragmentation and is characterized by a relatively flat ionization cross section for different classes of asphaltene molecules, thereby giving accurate mass distributions.[40,42,125,126] The inset shows that all asphaltenes are removed by the IR laser track going from upper left to lower right.

upon IR irradiation; there is no asphaltene left in the track made by the IR laser pulses moving from upper left to lower right. In addition, L^{2}MS data for a prepared mixture of several compounds with PAHs of various ring sizes, geometries, and compositions, including asphaltenes, showed that L^{2}MS signal amplitudes show a relatively invariant cross section.[42] Consequently, the various possible artifacts and inaccuracies of mass spectrometry applied to asphaltenes are minimized using L^{2}MS.

Figure 11 shows that an invariant mass distribution is obtained for asphaltenes independent of asphaltene surface concentrations and, thus, plume densities, laser powers, and laser pulse timing. These data show that artifacts of aggregation and fragmentation are not impacting the L^{2}MS molecular weight distributions. In contrast, it has been shown that "molecular" weight distributions from LDI MS are a function of laser power and asphaltene surface concentrations.[9,10] In

https://dx.doi.org/10.1021/acs.energyfuels.0c00874
Energy Fuels XXXX, XXX, XXX−XXX

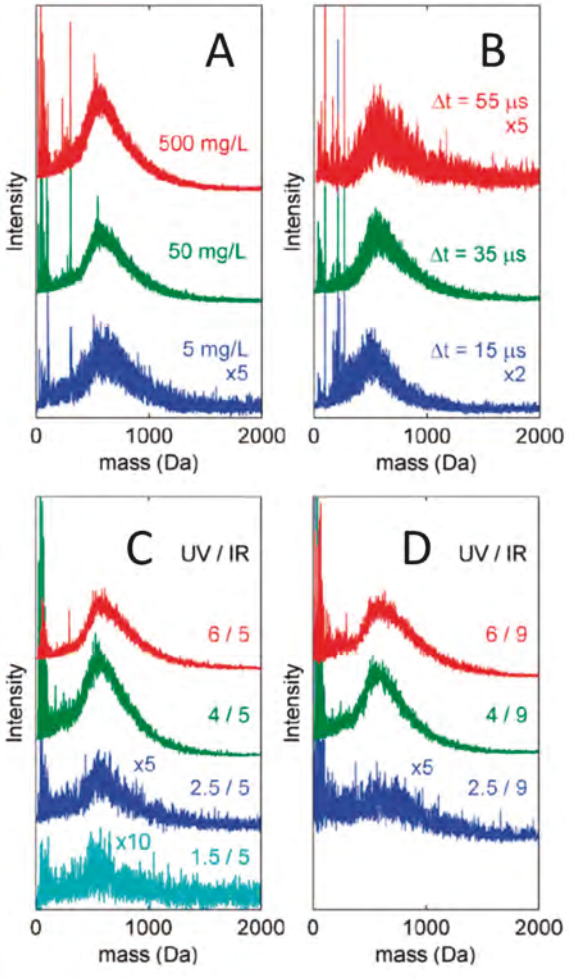

Figure 11. Typical L^2MS data for asphaltenes shows that the measured molecular weight distribution is independent of the (A) asphaltene surface concentration, (B) time between pulses, and (C and D) IR and UV laser power. Artifacts of aggregation at high plume densities and fragmentation at various higher laser powers are evidently not occurring; the asphaltene mass distribution is accurate.[13]

that case, low laser powers and surface concentrations are needed to minimize aggregation.[9,10] Consequently, L^2MS is robust for the application of molecular weight distributions.

L^2MS helped resolved apparent inconsistencies with LDI MS measurements. Some LDI MS measurements on asphaltenes gave lower molecular weights,[129] and some gave high molecular weights.[130] It was shown that LDI MS could give either low or high molecular weights based on how the instrument was tuned; high laser power gave high molecular weights.[9,34,131] Some argued that high laser power was necessary to volatize the heavy components of asphaltenes; hence, high molecular weights were correct. Others argued that high laser power caused aggregation; hence, low molecular weights were correct. The argument was settled by L^2MS, which is similar to LDI MS but strongly suppresses aggregation inherently. There, it was found the low molecular weights were obtained even under the highest laser powers attainable, thus confirming low molecular weights for asphaltenes.[12,13,41,42]

It is also important to validate that L^2MS does not suffer from unrecognized aggregation effects. If aggregates are not disaggregated, then these residual aggregates would evade or skew molecular weight determination. To measure the effect of aggregation, a gentle desorption method is used that contrasts L^2MS. SALDI MS employs an indirect heating of the sample;[40,49,60] the desorption process proceeds by the laser heating the substrate, which then heats the adsorbed asphaltene. Additionally, ionization occurs simultaneously with desorption and, therefore, at relatively high asphaltene density in the gas phase; this process allows aggregates to be held together by the ion-induced dipole interaction. Thus, indirect heating and prompt ionization can preserve weakly bound aggregates.

Figure 12 shows the application of SALDI MS on asphaltenes.[49] At the lowest laser powers, there is no signal.

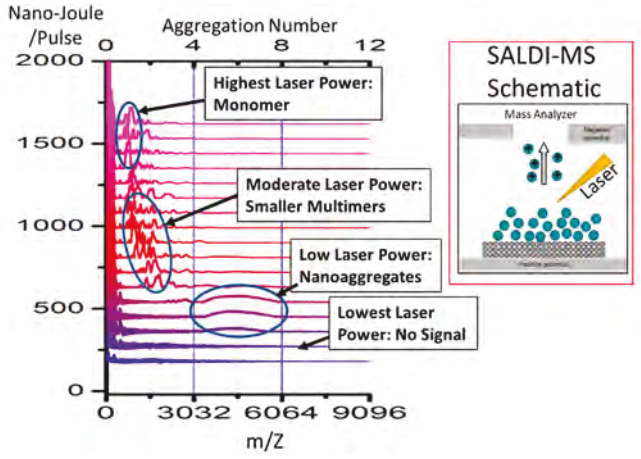

Figure 12. Application of a "gentle" desorption method to preserve nanoaggregates (SALDI MS).[40,49,60] At the lowest laser powers, there is no signal; there is too little desorption and ionization of asphaltenes. At low laser powers, nanoaggregates of asphaltenes are preserved and measured. At moderate laser power, asphaltene multimers are observed that are smaller than the nanoaggregate. At the highest laser powers, asphaltene molecules are observed. This establishes that asphaltene nanoaggregates can be disaggregated by laser desorption, even when using the gentle technique SALDI MS.

At low laser powers, the only signal is from nanoaggregates of aggregation number of ~7. With moderate laser power, multimers are detected. Smaller multimers are produced at higher laser energies. At the highest laser powers, asphaltene monomers are detected. These data show the expected result; it is difficult to preserve the weakly bound nanoaggregates in the desorption process.[40,49,60] The conclusion is that L^2MS, with its significantly more energetic desorption process than SALDI MS, completely disaggregates asphaltenes; thus, the L^2MS conclusions regarding asphaltenes apply to the entire asphaltene sample.

The conclusions from Figure 12 that asphaltene nanoaggregates are weakly bound can be compared to their solution properties. The critical nanoaggregate concentration of asphaltenes in toluene has been measured by many techniques, including high-Q ultrasonics,[53,54] NMR,[26,28−30] DC conductivity,[55,57] and centrifugation,[57,58] to be about 150 mg/L or 2×10^{-4} M.

$$\Delta G = -RT \ln([\mathrm{CNAC}]) \quad (5)$$

With eq 5, the nanoaggregate Gibbs free energy of aggregtation (ΔG) is ~5 kcal/mol, which is 5% of covalent bond strengths, despite being over an extended spatial area. In addition, the limited temperature dependence in the CNAC (concentra-

https://dx.doi.org/10.1021/acs.energyfuels.0c00874
Energy Fuels XXXX, XXX, XXX−XXX

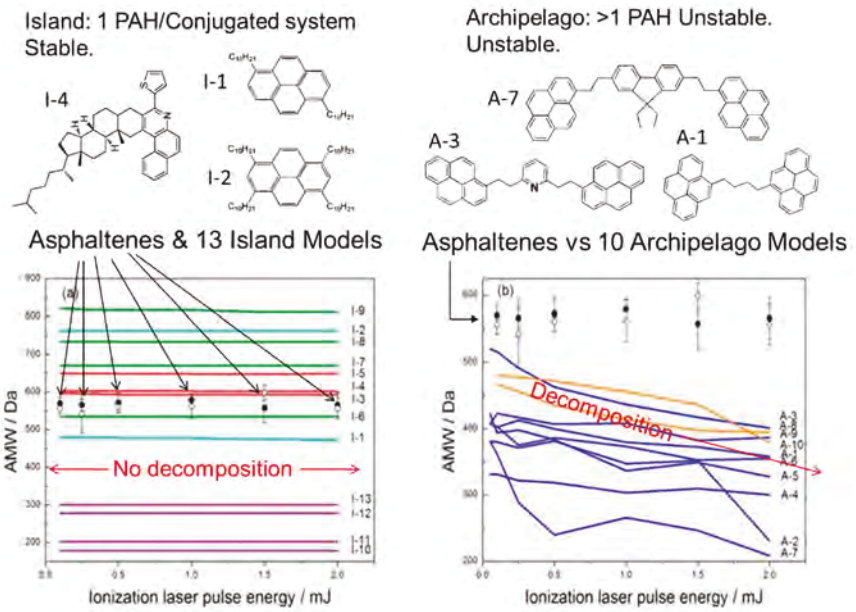

Figure 13. Average molecular weight (AMW) versus laser power for 23 model compounds and asphaltenes.[41] The structures of several island and archipelago model compounds are shown at the top and were evaluated by L^{2}MS. (Left) At higher UV laser power, island molecules and asphaltenes remain stable. (Right) However, under these same conditions, archipelago molecules with more the one PAH cross-linked with alkanes fragment; thus, their AMW decreases. This behavior is in contrast to asphaltenes. These results indicate that asphaltenes are dominated by island molecular architecture.[41] Note that a molecule with a direct aryl linkage (I-4) is defined here as an island structure because of its single network of sp^2-hybridized carbon.

tion)[26,57] means that a significant fraction of the Gibb's free energy of aggregate formation is entropic, which is typical, for example, for micelles. That is, for micelles, frequently, the entropy increase of the solvent is greater than the entropy decrease of the surfactant upon micelle formation.[132] Thus, the enthalpy of asphaltene nanoaggregate formation is even smaller than 5 kcal/mol. This small enthalpic value is consistent with aggregate and multimer dissociations observed in Figure 12. The CCC of asphaltenes in toluene is at higher concentrations than the CNAC and is about 4 g/L.[68,133,134] From eq 5, this corresponds to a aggregation free energy of ~3 kcal/mol. SALDI MS desorption is sufficiently gentle to preserve the nanoaggregate at low laser powers but does not preserve clusters because they are too weakly bound. As with nanoaggregates, the CCC is not very temperature-dependent; thus, the binding free energy has a considerable entropic component.[134] This lack of temperature dependence of both the CNAC and CCC helps explain why both nanoaggregates and clusters are found at elevated temperatures of 100 °C in oilfield reservoirs.[17]

■ ASPHALTENE MOLECULAR ARCHITECTURE BY L^{2}MS

In addition to the determination of molecular weight, L^{2}MS can be used to assess asphaltene molecular architecture as well. Under conditions used for Figure 11, fragmentation was not observed. However, if the ionizing laser pulse energy is increased sufficiently, then fragmentation can result depending upon molecular architecture.[41] With this unimolecular decomposition method, asphaltene molecular architecture can be probed. That is, at higher UV laser pulse energies than employed in Figure 11, fragmentation for certain labile molecules can be induced in L^{2}MS studies. This provides a means to evaluate asphaltene molecular architecture.

Figure 13 shows results from L^{2}MS studies designed to probe asphaltene molecular architecture. Unimolecular decomposition preferentially selects for less stable molecules, and this turns out to be key for asphaltenes. Of the 23 model compounds, half had a single aromatic core (island) and the other half had multiple aromatic cores cross-linked with alkane linkages (archipelago).[41] With higher ionization laser power, none of the island molecules nor the asphaltenes decompose, while, under the same conditions, all of the multicore molecules decompose. This instability of archipelago structures suggests a reason for their absence in asphaltenes; they fall apart. In these experiments, a molecule I-4 with structure shown in Figure 13 has a single core containing all aromatic carbon and two aromatic moieties connected by an aryl linkage. The authors labeled this molecule an island.[41] Others have labeled such molecules as archipelago.[47] We have proposed to designate this class of molecules as an "aryl-linked core" in the eponymous section below. Such a designation clarifies the true molecular structure and avoids a vestigial debate, which had been over significant differences (panel A versus panel B of Figure 8) but which has been reduced to more subtle differences (panel A versus panel C of Figure 8).

■ DEFINITION OF "ARYL-LINKED CORE"

We propose to avoid confusion by use of a third class of molecular architecture: molecules with an "aryl-linked core". This class has been defined as both island[41] and archipelago[47] and, thus, is a semantic problem and requires a new definition. This new classification "aryl-linked core" is to be added to the island and archipelago designations, aiding in establishing structure–function relations of asphaltenes. The "aryl-linked core" structure is defined as having a single, contiguous sp^2-hybridized carbon network containing one or more aryl

https://dx.doi.org/10.1021/acs.energyfuels.0c00874
Energy Fuels XXXX, XXX, XXX−XXX

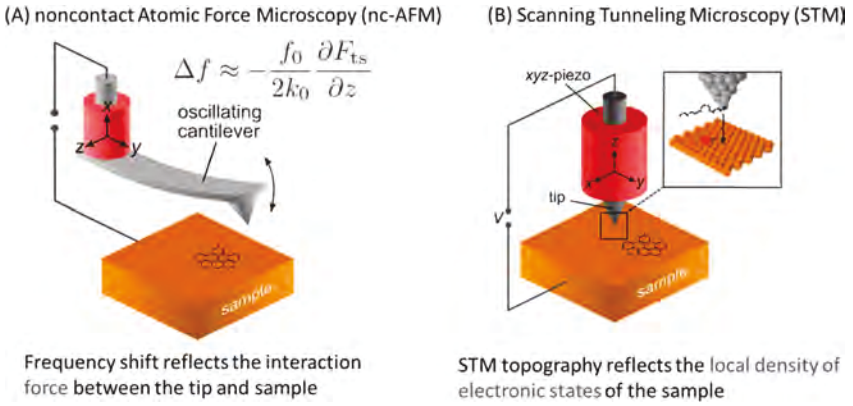

Figure 14. Schematic of the combined AFM and STM measurements.[47,48] (A) Schematic of the nc-AFM measurement; in the limit of small amplitudes, the frequency shift Δf is proportional to the vertical derivative of the force between the probe tip and the sample (F_{ts}). (B) STM imaging obtained by maintaining a constant current with deflections in height.

linkages, in which adjacent aromatic rings are directly bonded together but do not share a common bond in a ring. Examples of this aryl-linked core structure are shown in Figure 8C and in structure I-4 of Figure 13. In contrast, a traditional island structure also has a single, contiguous sp^2-hybridized carbon network but has adjacent aromatic rings exclusively fused (sharing a common bond in a ring) with no aryl linkages. Examples are shown in Figure 8A and structures I-1 and I-2 in Figure 13. The definition of archipelago remains unchanged and consists of multiple, discontinuous sp^2-hybridized carbon networks, in which these different aromatic ring systems are connected by one or more sp^3-hybridized carbons. An example of the archipelago structure is shown in Figure 8B.

AFM AND STM MOLECULAR IMAGING OF ASPHALTENES

About 10 years ago, real-space single-molecule imaging using non-contact atomic force microscopy (nc-AFM) emerged as a new tool for analytical chemistry.[135] Thereby the interaction force between a molecule adsorbed on a surface and a well-defined tip termination, such as a CO molecule, is measured (see Figure 14).[136,137] CO-tip nc-AFM has been used to probe the bond order[135] and aromaticity of molecules,[138,139] their adsorption geometry,[140] and conformations,[141,142] to determine moiety specific contrasts,[143,144] and to measure the intramolecular charge distribution.[145] Today, many groups worldwide have adapted this technique and are generating a growing library of characterized model compounds.

Moreover, nc-AFM can be readily combined with scanning tunneling microscopy (STM) by employing a qPlus quartz-crystal cantilever.[146] Using STM, frontier molecular orbitals of single molecules can be imaged,[147] providing a complementary electronic fingerprint. Both CO-tip nc-AFM and STM orbital imaging are most suited for planar, aromatic molecules.

CO-tip nc-AFM has also been applied for molecular structure identification[148] of purified natural compounds,[149] reaction products,[150,151] and molecular mixtures.[47,152,153] The single-molecule sensitivity and real-space character renders it particularly powerful for studying complex mixtures with a diverse set of *a priori* unknown molecules, such as asphaltenes.[47,48]

SETUP AND SAMPLE PREPARATION

The STM/AFM experiments are conducted in ultrahigh vacuum (UHV; $p \approx 1 \times 10^{-10}$ mbar) and low temperatures ($T \approx 6$ K). The cryogenic temperature completely suppresses thermal diffusion of the adsorbed molecules and, hence, prevents the formation of agglomerates or clusters. Under UHV conditions, the sample stays free from any contaminants over several weeks of measurements. For more details on the experimental setup, we refer to previous publications.[47,48]

Before the molecules are deposited, a clean surface of a metal single crystal, such as Cu(111), is prepared by sputtering and annealing cycles. Then, the bilayer of NaCl islands are grown that provide an electronic decoupling important for orbital measurements. AFM measurements, however, can be taken on both metallic Cu and ultrathin NaCl insulator. The molecules are deposited by two simple steps depicted in Figure 15. First, a couple of grains of the solid, dry material is placed on a piece of silicon wafer with a native oxide. Then, after transfer into ultrahigh vacuum, the silicon wafer is resistively flash-heated, causing the molecules to be sublimed from the wafer and, subsequently, collected on the sample surface at a low temperature (<10 K). Importantly, the sticking coefficient

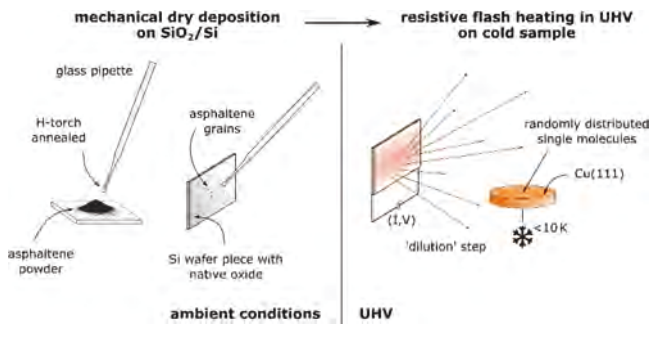

Figure 15. Schematic of asphaltene sample transfer for AFM and STM imaging.[47,48] Dry asphaltene powder was placed on a silicon wafer. In a high vacuum, flash heating desorbs the asphaltenes from the surface and ballistically transports them to a very cold surface (10 K); the low temperature assures that all asphaltenes stick. When checked, no asphaltene was found to remain on the flashed surface; therefore, all asphaltene is evaluated. Examination areas of the cold plate are randomly selected to preclude experimenter bias. In the many asphaltene imaging experiments, no asphaltene aggregates were found on the cold plate, only individual molecules.

https://dx.doi.org/10.1021/acs.energyfuels.0c00874
Energy Fuels XXXX, XXX, XXX−XXX

of any molecule is virtually unity at such low temperatures; consequently, any material that is sublimed will be collected. Many model compounds proved that thermal flash sublimation in vacuum is an effective and non-invasive way to volatilize molecules as large as 1000 amu, even if they comprise fragile bonds [see the "Archipelago Model Compounds (Not Found in Asphaltenes)" section below].[154] The rapid heating technique had been demonstrated to enhance volatility by favoring evaporation and suppressing competitive decomposition for various compounds.[155] The sample covers only a small solid angle of the isotropically evaporated molecules to "thin out" the concentration, such that isolated, randomly distributed molecules are observed on the sample surface. A low amount of CO molecules is co-adsorbed, which can be picked up by atomic manipulation to functionalize the tip.[137]

AFM AND STM IMAGES OF DIVERSE ASPHALTENES

A very diverse set of asphaltenes has been analyzed by ultrahigh-resolution AFM and STM.[47,48] For each sample, about 100 molecules have been imaged, which yields statistically relevant results. Because molecules are measured one by one, time constraints limit the number of molecules that can be practically analyzed. In this respect, the single-molecule detection that gives a significant edge over ensemble measurement techniques in molecule mixtures is both a blessing and a curse. Table 1 lists the origin of the asphaltene

Table 1. Source Material of Asphaltene Samples

PA	virgin petroleum
CA	asphaltene from hydroconverted coal tar resid
A1	asphaltene from virgin crude oil with deposition problems
A2	asphaltene from oil field asphaltene deposit from crude oil A1
B1	asphaltene from vacuum resid from a heavy oil
B2	asphaltene from hydroconverted product from B1
C1	asphaltene from steam cracker tar
C2	vacuum resid after asphaltene removal
D1	immature source rock asphaltene, Green River
D2	immature source rock asphaltene, Eagle Ford

and the corresponding label in the images, some of which are reproduced here. With such a diverse set of asphaltenes from ExxonMobil, Shell, Chevron, and Schlumberger, the structural motifs that have been identified from image analyses are expected to be broadly applicable to asphaltenes. First, some images are presented, and then these structural motifs are discussed.[47,48]

The exceptional resolution that can be achieved by AFM and STM is shown in Figure 16.[47] Individual atoms and bonds are evident in the AFM image of an asphaltene molecule. Eight six-membered rings are resolved. The methyl group at the top of the image is bright (that is more repulsive) because methyl hydrogens are slightly protruding out of the molecular plane. Individual frontier molecular orbital densities are selected by adjusting the tip−sample voltage to the respective molecular resonance.[47] Here, the measured density corresponding to the lowest unoccupied molecular orbital (LUMO) and calculated LUMO are in excellent agreement, confirming the structure assigned by the AFM images of this molecule.

Figure 17 shows a few, characteristic molecular structures from the diverse set of asphaltene samples reproduced from ref 48. The few exemplary images shown here already hint at the

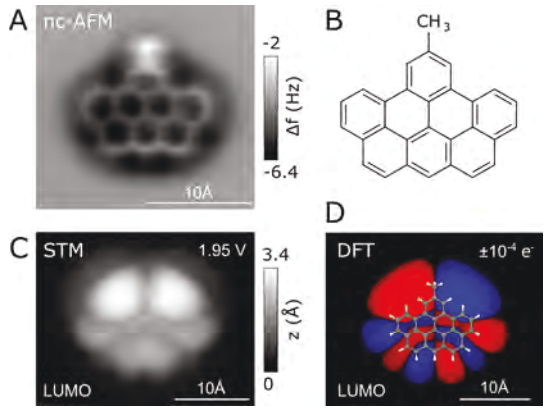

Figure 16. AFM and STM image of an asphaltene molecule.[47] (A) AFM image of atoms and bonds of the molecule. (B) PAH with eight aromatic rings and a peripheral methyl group can be identified. (C) STM image of the LUMO, corresponding to the isosurface of the respective orbital electron density. (D) Density functional theory (DFT) calculation of the LUMO wave function for this molecule. The excellent agreement between the theory and experiment confirms the assigned structure.[47]

tremendous variety of molecular structures found in each sample. While each molecule can be considered essentially unique, common structural motifs were identified. These motifs include an aromatic core that frequently comprises five-membered rings, often with a heteroatom. These five-membered rings are either fully conjugated PAHs (such as fluoranthene) or unconjugated as a PAH with CH_2 attached (such as fluorene).[154] Moreover, peripheral methyl groups, alkyl side chains, and cycloaliphatic moieties were observed. Importantly, the assigned structures cover the entire range in a carbon number versus double-bond equivalent spectrum determined by atmospheric pressure photoionization Fourier transform ion cyclotron resonance mass spectrometry (APPI FT-ICR MS).[48] This is a further indication that a representative set of molecules could be measured by AFM.

Figure 18 shows more exemplary asphaltene structures. It is often helpful to collect several AFM images at different tip−sample distances to resolve different parts of the molecule. PAHs adsorb in general closer to the sample surface and, consequently, require smaller tip−sample distances, whereas alkane chains are best resolved at farther distances (cf. left and right images in Figure 18E). Alkane chains also have many degrees of freedom and, hence, can adopt different conformations on the surface, which renders assigning their exact chemical structure challenging. PAHs on the other hand are comparably easy to probe by AFM because they are rigid and planar. PAH and aliphatic parts can also be discriminated by STM orbital density imaging because the frontier orbitals are confined to the PAH region alone, as seen in Figure 18D.

Occasionally, we also find two disjoint PAH moieties that are connected by a single aryl bond, such as CA16 in Figure 18. We designate such molecules as part of the newly proposed class of the "aryl-linked core" architecture. As discussed in the "Asphaltene Molecular Characterization and Its Change over Time" section, this new nomenclature should clarify that such types of molecules cannot be considered "island" or "archipelago" in the conventional sense (cf. Figure 8). In fact, the "aryl-linked core" architecture can be considered a blend of island- and archipelago-type molecules. In terms of electronic properties, the disjoint PAH topology has some

https://dx.doi.org/10.1021/acs.energyfuels.0c00874
Energy Fuels XXXX, XXX, XXX−XXX

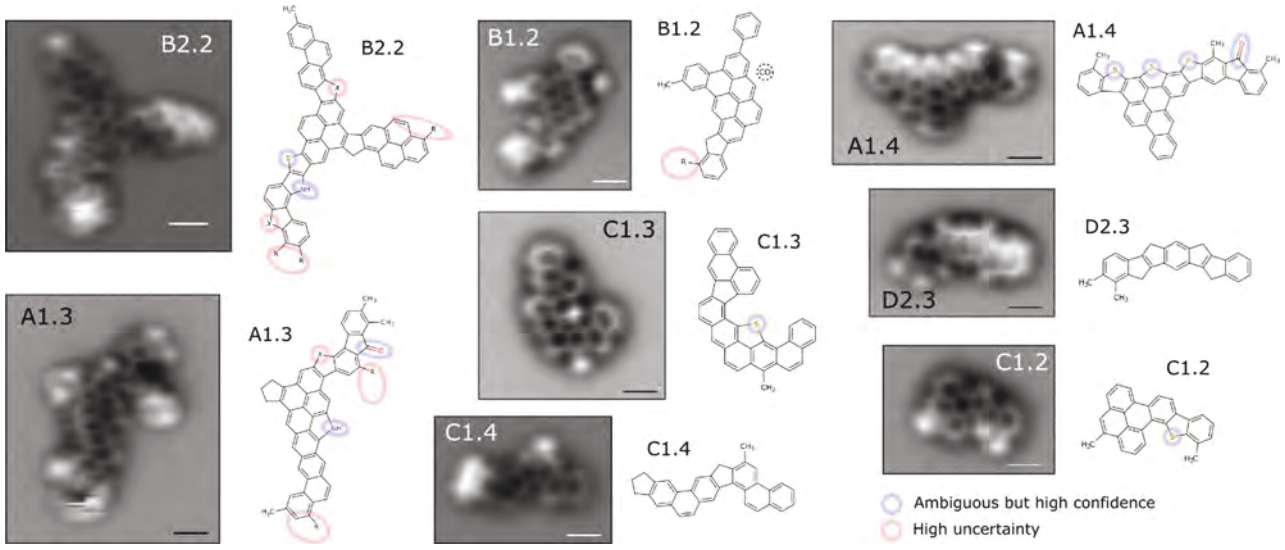

Figure 17. CO-tip AFM measurements and assigned structures from a diverse set of asphaltenes.[48] All molecules have a single core of aromatic carbon, generally with a single PAH. Occasionally, there is a single core containing all aromatic carbon of the molecule but with two or more aromatic groups bonded together with aryl linkages. The molecule designated B1.2 shows such an example with an aryl-linked phenyl group attached to the PAH. This structure we designate as an "aryl-linked core". Many molecules possess a five-membered ring often with a heteroatom. Red circles indicate moieties that cannot be identified unambiguously, and blue circles represent low uncertainty.

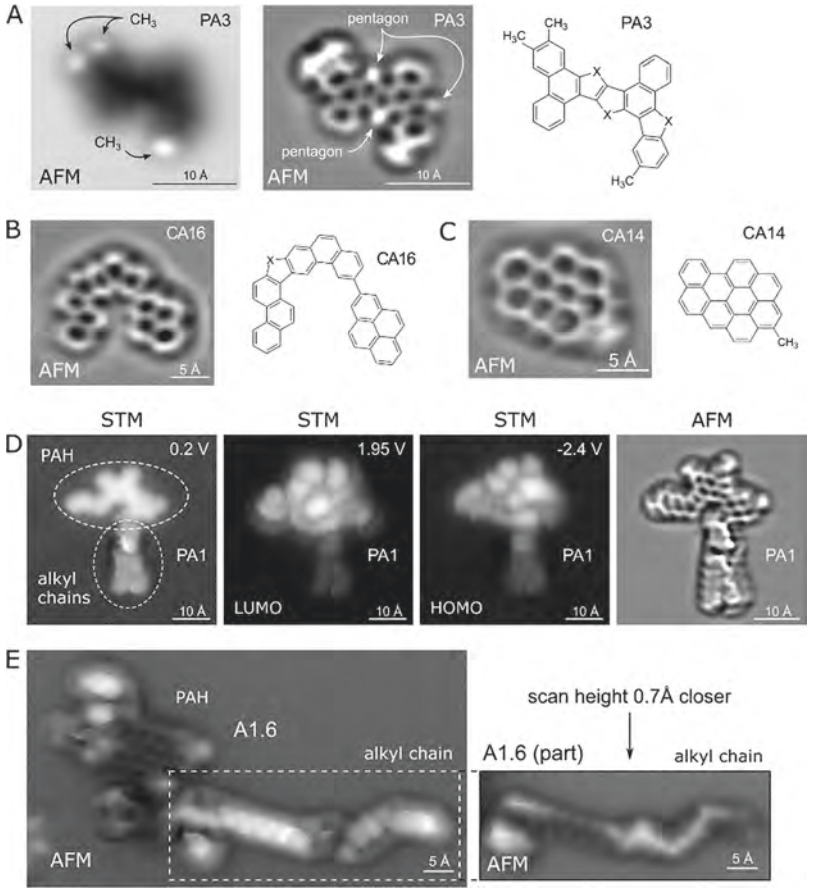

Figure 18. More AFM measurements and asphaltene molecular structures. Most of the structures are island with a single PAH core.[47,48] CA16 on the other hand features an aryl-linked pyrene group that we designate as an "aryl-linked core". Some molecules, such as PA1 and A1.6, have long alkane chains. Such aliphatic chains are clearly identified as such by their distinct zigzag pattern in AFM when they lie flat on the surface and by the absence of any orbital weight in STM images. STM imaging of molecular orbital densities also established that these molecules contained a single PAH. As with structures in Figure 17, five-membered rings are again very frequent.

https://dx.doi.org/10.1021/acs.energyfuels.0c00874
Energy Fuels XXXX, XXX, XXX−XXX

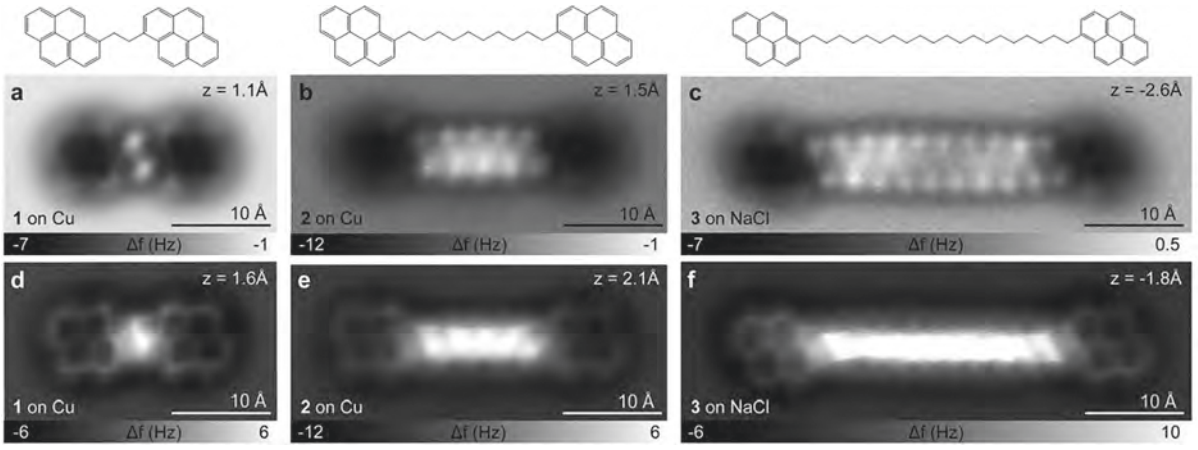

Figure 19. Three alkyldipyrenes, all archipelagos, were prepared to validate the AFM imaging protocol, especially flash-heating transfer, for such molecules.[142] This type of archipelago molecule, i.e., multiple PAH cores linked by an alkane chain, has not been observed in any asphaltene sample.[47,48] 1,2-Di(pyren-1-yl)ethane (BPE; MW = 430), 1,10-di(pyren-1-yl)decane (BPD; MW = 543), and 1,20-di(pyren-1-yl)icosane (BPI; MW = 683) were prepared and analyzed. The structures and corresponding AFM molecular images are shown. In the upper row, at a larger scan height, the alkyl chain is best resolved, whereas at a closer scan height (lower row), the PAH can be best identified. No fragmentation for any of these compounds was detected.[142] In particular, BPE has one of the weakest carbon−carbon bonds known at 65 kcal/mol (more typical is 88 kcal/mol in alkanes); even this bond did not break upon flash-heating transfer. BPI has a relatively large molecular weight, and the linking 20 carbon alkane chain could conceivably become entangled; nevertheless, no fragmentation was detected.

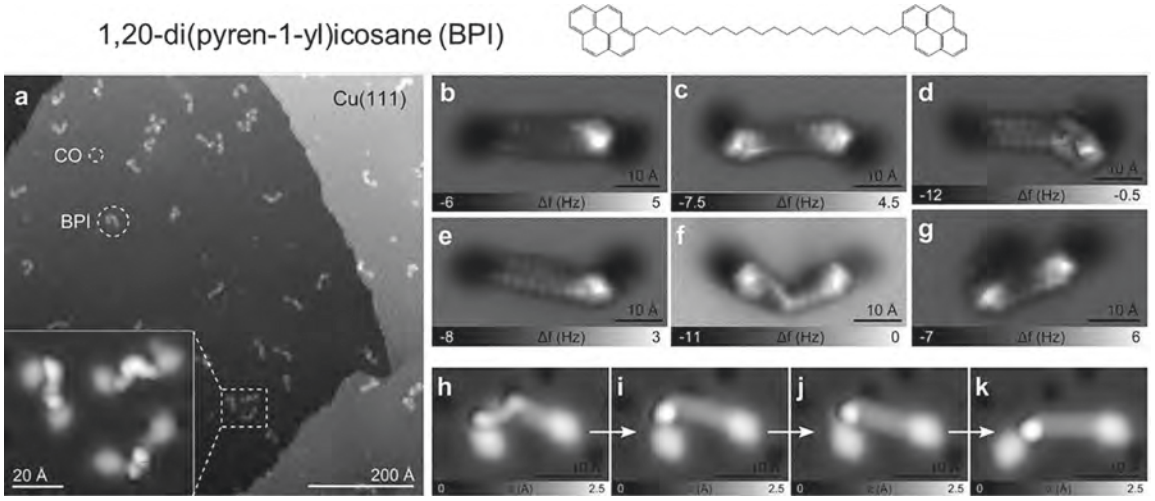

Figure 20. AFM and STM images of an alkyldipyrene, BPI (with its C20 linker), in many conformations.[142] (a) STM overview image of the BPI on Cu(111) sample preparation. Because of their structural degrees of freedom, BPI molecules exist in many different conformations on the surface. (b−g) Some conformations are shown in the CO-tip AFM images of BPI. (h−k) Conformation changes can be induced by voltage pulses (~3 V), as shown in the sequence of STM images (I = 2 pA and V = 0.2 V) after consecutive tip-induced conformation changes; by pushing one pyrene unit with the tip manipulation, the alkane linkage was extended but the twist remains.[142]

degree of conjugation dependent upon the relative orientation of the aromatics. Mechanically or sterically the molecules are expected to exhibit more similarities to single PAH molecules. While two aryl-liked PAHs can rotate against each other, they can, for instance, not fold over. Hence, they are expected to express the same type of hierarchical assembly behavior as described in the Yen−Mullins model. The "aryl-linked core" represents only a minority fraction of molecules measured in all samples. Moreover, for the 10 diverse asphaltenes listed in Table 1, for the hundreds of molecular images analyzed, the authors did not observe any conventional archipelago molecules.

ARCHIPELAGO MODEL COMPOUNDS (NOT FOUND IN ASPHALTENES)

The lack of observation of a single archipelago structure gave rise to concerns that perhaps such a molecular architecture would fragment in the flash-heating transfer depicted in Figure 15. Archipelago model compounds were designed, prepared, and subjected to the identical sample transfer process as the 10 asphaltene samples.[142] Figure 19 shows three structures that we refer to colloquially as alkyldipyrene compounds and the corresponding AFM images.

Figure 19 shows that all three of the alkyldipyrenes tested survived flash-heating transfer. The alkyl chain that connects the two pyrene units can be identified by its characteristic zigzag pattern (each kink is a methylene moiety) in AFM in its flat conformation. The compound BPE was included as a very

https://dx.doi.org/10.1021/acs.energyfuels.0c00874
Energy Fuels XXXX, XXX, XXX−XXX

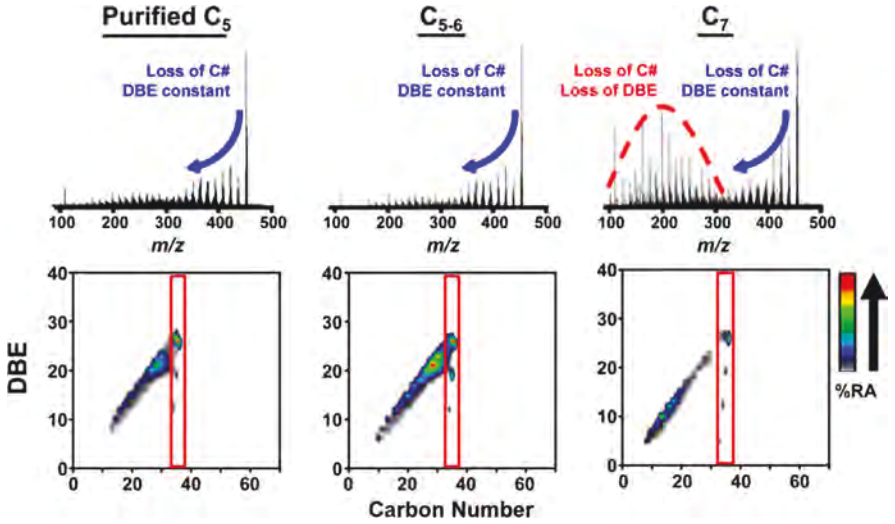

Figure 21. IRMPD of "purified" or fractionated asphaltenes (where a fraction of predominantly island molecules was removed).[158] For the asphaltenes isolated with *n*-pentane, there is little loss of double bond equivalent (DBE), which is defined as double bonds plus rings, after IRMPD; aromatic moieties are high in DBE. For these "purified" asphaltenes, there is a fraction of population (as shown) where, upon IR irradiation, the molecule cleaves into two fractions of roughly equal mass and where each fragment has a lower DBE than the original molecule. This result indicates separation of aromatic moieties upon dissociation, consistent with the presence of two aromatic moieties in the molecule. Two questions remain: (1) What structures give rise to this signal? (2) What is the magnitude of this fraction?

stringent test because the carbon−carbon bond energy between the two ethane carbons in this compound is very low at only 65 kcal/mol.[142] This bond should be particularly susceptible to breaking. Nevertheless, no fragmentation was observed in the same flash-heating and sample-capture process as used for the asphaltenes. In addition, BPI could have fragmented in this process because it has a relatively high molecular weight of 684 amu and has a long chain with two pyrene anchors at the ends that might become entangled with other molecules in the bulk and fragment upon heating. Nevertheless, BPE, BPD, and BPI showed no evidence of fragmentation.[142] The AFM and STM studies of diverse asphaltenes did not find archipelagos, indicating that they are not present in an appreciable concentration in asphaltenes. Such archipelagos might be present in small fractions in asphaltenes, which would be detectable by sensitive or selective methods.

Figure 20 shows a wider field of view for evaluation of the alkyldipyrene compound BPI, demonstrating the robust ability to image this and other compounds.[142] As mentioned previously, alkane chains exist in many different conformations on the surface as a result of their structural degrees of freedom (rotation and folding). Some conformations of BPI are shown in panels b−g of Figure 20. This renders their clear identification challenging, unless they are completely stretched out and adapt a planar geometry, as shown in Figure 19. However, conformational changes of alkane chains can be induced by voltage pulses from the tip (see panels h−k of Figure 20). It turns out that a flat geometry is often favored and eventually achieved, unless the pyrene units were "twisted" against each other at the time of adsorption. Through conformational changes, we can resolve different parts of the chain and it provides another way to identify aliphatic chains.

The lack of observation of even a single archipelago molecule of the sort in Figures 19 and 20 in 10 diverse asphaltene samples relegates this structural motif to a small mass fraction. The AFM and STM imaging results do show a secondary fraction of the molecular population of some asphaltenes with an aryl-linked core.[47,48] In a more recent study on petroleum pitch M-50, a number (4) of molecules with an aryl linkage or short linkers with C1−C3 between two aromatic cores were characterized by AFM and confirmed by model compounds.[153] This study again confirmed that these molecules can be imaged with this technique if they are present. In addition, this type of compound might be expected in thermally treated samples, albeit still in small quantify, which is consistent with the pyrolytic formation of archipelagos in earlier studies.[119] These results are consistent with the L^2MS results[41] and other mass spectral results[36] discussed earlier in Figure 13. Both measurements, AFM imaging and L^2MS, have relatively flat cross sections for analysis, independent of the molecular structure or weight within the asphaltenes. The agreement of these very different methods is reassuring. These results are also in agreement with the TRFD results discussed earlier (Figure 9);[5,6] however, while TRFD was the first technique to suggest an island architecture, it does not have a flat cross section for different asphaltene molecular populations.

■ ULTRAHIGH-RESOLUTION DISSOCIATION STUDIES

Recent studies employing APPI FT-ICR MS coupled with infrared multiphoton dissociation (IRMPD) have explored asphaltene molecular weight and architecture.[156−158] The relationship of these studies to other studies presented above has been discussed elsewhere.[17] The molecular weights obtained in these and other ultrahigh-resolution studies are broadly consistent with those obtained by a suite of other methods. These measurements also rule out dominance of the archipelago molecular structure of the sort originally proposed and presented in Figure 8B.[156−158] Moreover, the ultrahigh-resolution studies also are consistent with a substantial fraction of island structures in asphaltenes. Nevertheless, these studies also found a fraction of asphaltene molecules that have what the authors termed "archipelago" structures, which explicitly include a variety of structures, including molecules with a

https://dx.doi.org/10.1021/acs.energyfuels.0c00874
Energy Fuels XXXX, XXX, XXX−XXX

possible aryl-linked core and molecules with alkyl-linked PAHs.[156−158] These different structural classes were not differentiated in these studies. Figure 21 shows an example of these findings.

Figure 21 shows results from an ultrahigh-resolution mass spectral analysis of asphaltenes.[158] The methods used here have very high sensitivity to detection of components present, even in very small quantities.[159] However, the authors note that these methods employed have extreme sensitivity to aggregation with very large variations in cross section of a factor of 50 or more for reasons of uncertain origin.[156−158] In addition, ICR methods have inherent cross-section variability, especially for organic matter.[160] Consequently, quantitative mass fraction assessment is hindered.

The type of binding of the fragments in the initial molecule was not established in these studies.[156−158] No differentiation was made whether the fragments were originally linked with an alkane chain (archipelago) or with a direct aryl bond (aryl-linked core), but in these studies, all possible structures were labeled archipelago (thus would include the very different structures of panels B and C of Figure 8). In particular, the data in Figure 21 shows a splitting of molecules into roughly two equal parts but not, for example, 10 parts. Indeed, the small molecular weight of the original molecular population (~400 amu) is not compatible with fragmentation into many parts of an archipelago of the sort in Figure 8B.

The molecular AFM imaging of asphaltenes and the model compounds alkyldipyrenes addressed exactly the case of archipelago molecules that can naturally fragment into two roughly equal parts.[142] The mass range of 400 amu for asphaltenes in Figure 21 is well within the molecular weight range for efficient transfer and detection by AFM. Figures 19 and 20 show excellent sensitivity of AFM and STM imaging for detection of archipelago molecules with two PAHs cross-linked by an alkane chain. The AFM and STM studies of 10 diverse asphaltene samples showed no evidence of such archipelago molecules. Given this fact, then the interpretation of the data in Figure 21 is that the fragmenting molecules, if present in any significant quantity, are not likely to have two PAHs cross-linked by an alkane (archipelago) but are plausibly from an aryl-linked core. The 50× variation in cross section of the APPI FT-ICR MS studies makes direct comparisons somewhat uncertain.[156−158] The large, flat cross section and high efficiency of the AFM and STM imaging for detection of specific structures is a significant benefit for interpretation results of wide-ranging methods.

RHEOLOGICAL IMPLICATIONS OF MOLECULAR ARCHITECTURE

From a rheological standpoint, there is an important distinction between the island and aryl-linked core architectures on the one hand and archipelago architecture on the other hand. Asphaltenes are dominated by aromatic and saturated carbon. Aromatic carbon is characterized by stronger intermolecular interactions than saturated carbon as a result of its greater polarizability.[161] Heteroatoms can contribute to intermolecular interactions as well, in part as a result of some degree of dipole moment in corresponding chemical moieties. The most prevalent heteroatom is sulfur, which is generally found in nonpolar moieties of sulfides and thiophenes.[162,163] Frequently, the thiophene fraction dominates and is all associated with aromatic carbon. The next most abundant heteroatom is generally nitrogen. All nitrogen in asphaltenes is contained in aromatic functions.[164] Much oxygen in asphaltenes is also associated with the aromatic core.[165] Thus, the location of nitrogen and much sulfur and oxygen strengthens the intermolecular PAH interactions. The island and aryl-linked core architectures have predominantly one extended binding site per molecule, while the archipelago architecture has multiple binding sites. The single binding site of the island and aryl-linked core architectures lends itself toward nanoaggregate formation with small aggregation numbers. A disordered π stack can form, while the steric repulsion of peripheral alkanes helps limit aggregation numbers. Exactly such a structure for the nanoaggregate has been determined from combined SAXS and SANS.[61−63] X-ray scattering is enhanced by the presence of the high electron density of aromatic carbon, while neutron scattering is enhanced by the hydrogen content of saturated carbon. The separation of the absolute SAXS and SANS cross sections at 14 Å length scale and smaller showed the size of the nanoaggregate as well as the nanoaggregate structure with the central aromatic core. This structure is expected given the relative strengths of intermolecular interactions of aromatic versus alkane carbon.

The effect of asphaltenes on viscosity has been of great industrial interest for road paving and coating of materials. As shown in Figure 22, asphaltenes impart huge viscosity to

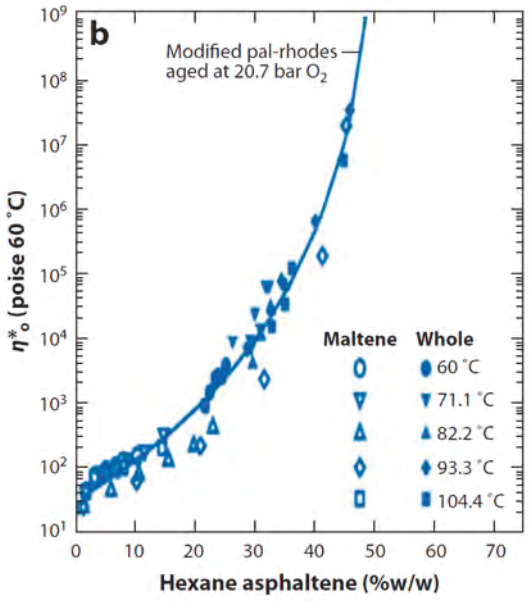

Figure 22. Viscosity versus asphaltene content.[166] Viscosity varies more than exponentially on the asphaltene content. This variation is accurately accounted for by models, such as a (modified) Pal−Rhodes model, that treat asphaltenes as dispersed colloidal particles in a solvent.[166,167]

carbonaceous materials but only at very high concentrations, such as tens of percent mass fraction.[166] Viscosity models that are used to account for and fit the change of viscosity with the change of asphaltene content, such as the Pal−Rhodes model,[168] use a colloidal model (consistent with nanoaggregates or clusters) of asphaltenes in a solvent.[166,167,169,170] These colloidal models apply for huge variations of the asphaltene content and huge variations of viscosity, as shown in Figure 22.[166] Thus, these huge rheological variations are consistent with the nanocolloidal structure of asphaltenes,

https://dx.doi.org/10.1021/acs.energyfuels.0c00874
Energy Fuels XXXX, XXX, XXX−XXX

which, in turn, are consistent with the molecular structure of the island and aryl-linked core architectures.

In contrast, asphaltenes do not form gels at a low concentration. It is well-known that gel formation is strongly associated with some form of cross-linking with individual molecules, each with multiple binding sites, and that gels form at low concentrations of these cross-linking components, giving very non-Newtonian viscosity behavior.[171] For example, the cross-linking polysaccharide used in agarose gel for gel electrophoresis is typically used in the weight/weight concentration range of 0.5−2%, depending upon the desired gel pore size.[172] Agarose gels are even used in concentrations as low as 0.1%, but these gels are fragile.[173] The rheological impact of asphaltenes at these concentrations is minimal. The formalisms to treat gel rheology[174,175] are fundamentally different from those that treat colloidal suspensions.

CONCLUSION

The resolution of asphaltene nanostructures has enabled broad application in fulfillment of Cricks' axiom, "to understand function, study structure". The dominant asphaltene molecular and nanocolloidal structures have been largely resolved. Effective centroids of the respective distributions are represented in the Yen−Mullins model. This model has been shown to provide a foundation for the thermodynamic treatment of asphaltene gradients in reservoir crude oils for reservoirs with length scales up to 100 km. This approach has been so effective that it has led to a new discipline, RFG, which has been employed for understanding a myriad of characteristics of oilfield reservoirs. Specifically, the asphaltene thermodynamic treatment allows for the determination of when reservoir fluids are equilibrated. Equilibrated fluids imply flow connectivity in reservoirs addressing often the most important risk factor in production. Disequilibrium of reservoir fluids is often associated with identifiable fluid processes that preclude equilibrium. A collection of such processes defines RFG. Characterization of the evolution of reservoir fluids is always found to improve the understanding of the reservoir realization. Another application of improved asphaltene molecular characterization is the consistent treatment of the oil−water interface with the Langmuir equation of state. Dependent upon the application, some interfacial properties can be characterized simply by use of the centroid of the asphaltene distribution, while other interfacial properties are characterized by a first-order correction to the asphaltene molecular characterization. In addition, rheological properties are consistent with the asphaltene molecular and colloidal structures discussed herein.

The asphaltene molecular weight and molecular architecture had been the subject of a substantial debate, with variations in chemical properties that differed by a factor of 10 or more (cf. panel A versus panel B of Figure 8). The cause of the debates stemmed largely from unrecognized aggregation. Indeed, in solution and crude oils, the asphaltenes exhibit three solubility thresholds and not just one, which is more typical of a solute−solvent system. Literature arguments followed as a result of the erroneous assignment of aggregate properties to molecules.

Consistent results from the various analyses described here demonstrate that the average mass of asphaltene molecules is close to 700 or 750 amu. This result alone excludes the historically recognized model of archipelago asphaltenes, as in Figure 8B, because molecules with many fused ring systems must have significantly higher molecular weight. Nevertheless, debate over the significance of island versus archipelago structures persisted after consensus regarding molecular weight was achieved. Later, the term archipelago was redefined from meaning alkyl cross-linking of many aromatic cores to meaning cross-linking a few or just two aromatic cores. Applications of many sophisticated methods for the evaluation of asphaltenes (such as TRFD, L^2MS, AFM, and STM) have reduced the chemical uncertainties substantially, with the asphaltene structure now shown to be dominated by single aromatic core systems, in which that core is typically fully fused (island) and occasionally contains one or, on rare occasions, more direct aryl linkages (now called aryl-linked core), e.g., panel A versus panel C of Figure 8. Archipelagos have not been detected with sensitive methods in a diverse set of asphaltenes. Model archipelago compounds were prepared and analyzed to validate corresponding detection methodologies. In large measure, the remaining uncertainties are at the level of refinement of structures and molecular weights that contributes to asphaltenes. A cautionary note is that, while the chemical uncertainties of asphaltenes have been greatly diminished, the language of the original, substantial debate has been retained, with some confusing shifts in definitions over time. Herein, we propose to mitigate confusion by clarifying the language particularly of the dominant molecular structures that contribute to asphaltenes. In particular, for asphaltenes, (1) the island structure with a single PAH is prominent and generally found to be dominant in 10 diverse asphaltene samples from different source materials, some of which were subject to various chemical processes, (2) molecules with an aryl-linked core contribute to some degree (defined in the eponymous section), and (3) and the archipelago structure (with PAHs cross-linked with alkane chains) appears to contribute a minor amount or not at all to asphaltenes.

From an aggregation standpoint, both the island and aryl-linked core structures have predominantly a single intermolecular binding site per molecule; that structure is consistent with the observed asphaltene behavior of forming nanoaggregates but not gels at low concentrations. Simple rheologic models of asphaltenes, such as the Pal−Rhodes model, are consistent with the colloidal model of asphaltenes discussed herein. In contrast, the archipelago structure has multiple binding sites per molecule, which is consistent with gel formation, contrary to asphaltene behavior. In addition, to cleave aromatics off the molecule, the island structure requires cleaving multiple aromatic bonds, the aryl-linked core structure requires cleaving one aryl bond, and the archipelago structure requires cleaving an alkyl bond. Because the dominant (island) and secondary (aryl-linked core) structures present in asphaltenes have predictable properties, the asphaltene molecular structures are considered reasonably well-understood.

AUTHOR INFORMATION

Corresponding Author

Oliver C. Mullins − *Schlumberger-Doll Research, Cambridge, Massachusetts 02139, United States;* orcid.org/0000-0001-6951-9415; Email: mullins1@slb.com

Authors

Bruno Schuler − *IBM Research−Zurich, 8803 Rüschlikon, Switzerland*

https://dx.doi.org/10.1021/acs.energyfuels.0c00874
Energy Fuels XXXX, XXX, XXX−XXX

Yunlong Zhang − *ExxonMobil Research and Engineering Company, Annandale, New Jersey 08801, United States*
Fang Liu − *Energy Institute and Department of Chemical Engineering, City College of New York, New York City, New York 10031, United States*
Andrew E. Pomerantz − *Schlumberger-Doll Research, Cambridge, Massachusetts 02139, United States;* orcid.org/0000-0003-2639-2682
A. Ballard Andrews − *Schlumberger-Doll Research, Cambridge, Massachusetts 02139, United States*
Leo Gross − *IBM Research−Zurich, 8803 Rüschlikon, Switzerland;* orcid.org/0000-0002-5337-4159
Vincent Pauchard − *Energy Institute and Department of Chemical Engineering, City College of New York, New York City, New York 10031, United States;* orcid.org/0000-0003-1027-4526
Sanjoy Banerjee − *Energy Institute and Department of Chemical Engineering, City College of New York, New York City, New York 10031, United States*

Complete contact information is available at: https://pubs.acs.org/10.1021/acs.energyfuels.0c00874

Notes

The authors declare no competing financial interest.

NOMENCLATURE

AFM = atomic force microscopy
AMW = average molecular weight
APCI = atmospheric pressure chemical ionization
APPI FT-ICR MS = atmospheric pressure photoionization Fourier transform ion cyclotron resonance mass spectrometry
BPD = 1,10-di(pyren-1-yl)decane
BPE = 1,2-di(pyren-1-yl)ethane
BPI = 1,20-di(pyren-1-yl)icosane
C_b = bulk concentration
CCC = critical cluster concentration
CNAC = critical nanoaggregate concentration
C_{si} = subsurface concentration of component i
D = diffusion constant
DBE = double bond equivalent
DFT = density functional theory
DFA = downhole fluid analysis
η^* = zero shear rate complex dynamic viscosity
δ = Hildebrand solubility parameter of the oil
δ_a = Hildebrand solubility parameter of the asphaltenes
$\Delta\rho$ = density difference between asphaltenes and the oil phase
$\Delta\gamma_{eq}$ = reduction of surface tension at equilibrium
ΔG = difference in Gibbs free energy
EoS = equation of state
ESI FT-ICR MS = electrospray ionization Fourier transform ion cyclotron resonance mass spectrometry
FHZ EoS = Flory−Huggins−Zuo equation of state
$\varphi_a(h_i)$ = volume fraction of asphaltene in the crude oil at height h_i
g = Earth's gravitational acceleration
GOR = gas−oil ratio
γ_o = clean surface interfacial tension
$\gamma(\Gamma)$ = interfacial tension
Γ = surface coverage
Γ_∞ = maximum surface coverage
h = height in the oil column
HOMO = highest occupied molecular orbital
IFT = interfacial tension
IRMPD = infrared multiphoton dissociation
k = Boltzmann constant
k_i = adsorption constant of component i
K_H = Henry's law constant
LDI MS = laser desorption ionization mass spectrometry
LIAD MS = laser-induced acoustic desorption mass spectrometry
LUMO = lowest unoccupied molecular orbital
L^2MS = laser desorption, laser ionization mass spectrometry
λ = wavelength
MW = molecular weight
ncAFM = non-contact atomic force microscopy
OD = optical density
PAH = polycyclic aromatic hydrocarbon
Π = surface pressure
R = universal gas constant
RFG = reservoir fluid geodynamics
ρ = oil density
ρ_a = asphaltene density
SALDI MS = surface-assisted laser desorption/ionization mass spectrometry
SANS = small-angle neutron scattering
SAXS = small-angle X-ray scattering
SFG = sum frequency generation
STM = scanning tunneling microscopy
T = temperature
TRFD = time-resolved fluorescence depolarization
TVDss = true vertical depth subsea
τ = time
τ_D = characteristic diffusion time
θ_i = fractional surface coverage
V = volume (of the relevant asphaltene species)
VPO = vapor pressure osmometry
v = molar volume of oil
v_a = molar volume of the relevant asphaltene species

REFERENCES

(1) *Asphaltenes, Heavy Oils, and Petroleomics*; Mullins, O. C., Sheu, E. Y., Hammami, A., Marshall, A. G., Eds.; Springer: New York, 2007; DOI: 10.1007/0-387-68903-6.
(2) *Structures and Dynamics of Asphaltenes*; Mullins, O. C., Sheu, E. Y., Eds.; Springer: Boston, MA, 1998; DOI: 10.1007/978-1-4899-1615-0.
(3) *Asphaltenes and Asphalts, 2*; Yen, T. F., Chilingarian, G. V., Eds.; Elsevier: Amsterdam, Netherlands, 2000.
(4) *Chemistry of Asphaltenes*; Bunger, J. W., Li, N. C., Eds.; American Chemical Society (ACS): Washington, D.C., 1982; Advances in Chemistry, Vol. *195*, DOI: 10.1021/ba-1981-0195.
(5) Groenzin, H.; Mullins, O. C. Asphaltene Molecular Size and Structure. *J. Phys. Chem. A* **1999**, *103*, 11237−11245.
(6) Groenzin, H.; Mullins, O. C. Molecular Size and Structure of Asphaltenes from Various Sources. *Energy Fuels* **2000**, *14*, 677−684.
(7) Marshall, A. G.; Rodgers, R. P. Petroleomics: Chemistry of the underworld. *Proc. Natl. Acad. Sci. U. S. A.* **2008**, *105* (47), 18090−18095.
(8) Rodgers, R. P.; Marshall, A. G. Petroleomics: Advanced characterization of petroleum-derived materials by Fourier transform ion cyclotron resonance mass spectrometry (FT-ICR MS). In *Asphaltenes, Heavy Oils, and Petroleomics*; Mullins, O. C., Sheu, E. Y., Hammami, A., Marshall, A. G., Eds.; Springer: New York, 2007; pp 63−93, DOI: 10.1007/0-387-68903-6_3.

(9) Hortal, A. R.; Hurtado, P.; Martínez-Haya, B.; Mullins, O. C. Molecular Weight Distributions of Coal and Petroleum Asphaltenes from Laser Desorption/Ionization Experiments. *Energy Fuels* **2007**, *21*, 2863−2868.
(10) Hortal, A. R.; Martínez-Haya, B.; Lobato, M. D.; Pedrosa, J. M.; Lago, S. On the determination of molecular weight distributions of asphaltenes and the aggregates in laser desorption ionization experiments. *J. Mass Spectrom.* **2006**, *41*, 960−968.
(11) Mullins, O. C.; Martinez-Haya, B.; Marshall, A. G. Contrasting Perspective on Asphaltene Molecular Weight. This Comment vs the Overview of A. A. Herod, K. D. Bartle, and R. Kandiyoti. *Energy Fuels* **2008**, *22*, 1765−1773.
(12) Pomerantz, A. E.; Hammond, M. R.; Morrow, A. L.; Mullins, O. C.; Zare, R. N. Two-Step Laser Mass Spectrometry of Asphaltenes. *J. Am. Chem. Soc.* **2008**, *130*, 7216−7217.
(13) Pomerantz, A. E.; Hammond, M. R.; Morrow, A. L.; Mullins, O. C.; Zare, R. N. Asphaltene Molecular-Mass Distribution Determined by Two-Step Laser Mass Spectrometry. *Energy Fuels* **2009**, *23*, 1162−1168.
(14) Mullins, O. C. The Modified Yen Model. *Energy Fuels* **2010**, *24*, 2179−2207.
(15) Mullins, O. C.; Sabbah, H.; Eyssautier, J.; Pomerantz, A. E.; Barré, L.; Andrews, A. B.; Ruiz-Morales, Y.; Mostowfi, F.; McFarlane, R.; Goual, L.; et al. Advances in Asphaltene Science and the Yen−Mullins Model. *Energy Fuels* **2012**, *26* (7), 3986−4003.
(16) Zuo, J. Y.; Mullins, O. C.; Freed, D.; Elshahawi, H.; Dong, C.; Seifert, D. J. Advances in the Flory−Huggins−Zuo Equation of State for Asphaltene Gradients and Formation Evaluation. *Energy Fuels* **2013**, *27*, 1722−1735.
(17) Mullins, O. C. *Reservoir Fluid Geodynamics and Reservoir Evaluation*; Schlumberger: Houston, TX, 2019.
(18) Freed, D. E.; Mullins, O. C.; Zuo, J. Y. Theoretical Treatment of Asphaltene Gradients in the Presence of GOR Gradients. *Energy Fuels* **2010**, *24* (7), 3942−3949.
(19) Buch, L.; Groenzin, H.; Buenrostro-Gonzalez, E.; Andersen, S. I.; Lira-Galeana, C.; Mullins, O. C. Molecular size of asphaltene fractions obtained from residuum hydrotreatment. *Fuel* **2003**, *82* (9), 1075−1084.
(20) Groenzin, H.; Mullins, O. C.; Eser, S.; Mathews, J.; Yang, M.-G.; Jones, D. Molecular size of asphaltene solubility fractions. *Energy Fuels* **2003**, *17* (2), 498−503.
(21) Buenrostro-Gonzalez, E.; Groenzin, H.; Lira-Galeana, C.; Mullins, O. C. The Overriding Chemical Principles that Define Asphaltenes. *Energy Fuels* **2001**, *15*, 972−978.
(22) Wargadalam, V. J.; Norinaga, K.; Iino, M. Size and shape of coal asphaltene studied by viscosity and diffusion coefficient measurement. *Fuel* **2002**, *81*, 1403−1407.
(23) Andrews, A. B.; Guerra, R. E.; Mullins, O. C.; Sen, P. N. Diffusivity of Asphaltene Molecules by Fluorescence Correlation Spectroscopy. *J. Phys. Chem. A* **2006**, *110*, 8093−8097.
(24) Andrews, A. B.; Shih, W.-C.; Mullins, O. C.; Norinaga, K. Molecular size determination of coal-derived asphaltene by fluorescence correlation spectroscopy. *Appl. Spectrosc.* **2011**, *65* (12), 1348−1356.
(25) Guerra, R. E.; Ladavac, K.; Andrews, A. B.; Mullins, O. C.; Sen, P. N. Diffusivity of coal and petroleum asphaltene monomers by fluorescence correlation spectroscopy. *Fuel* **2007**, *86*, 2016−2020.
(26) Lisitza, N. V.; Freed, D. E.; Sen, P. N.; Song, Y.-Q. Study of Asphaltene Nanoaggregation by Nuclear Magnetic Resonance (NMR). *Energy Fuels* **2009**, *23*, 1189−1193.
(27) Freed, D. E.; Lisitza, N. V.; Sen, P. N.; Song, Y.-Q. Molecular Composition and Dynamics of Oils from Diffusion Measurements. In *Asphaltenes, Heavy Oils, and Petroleomics*; Mullins, O. C., Sheu, E. Y., Hammami, A., Marshall, A. G., Eds.; Springer: New York, 2007; pp 279−299, DOI: 10.1007/0-387-68903-6_11.
(28) Rane, J. P.; Harbottle, D.; Pauchard, V.; Couzis, A.; Banerjee, S. Adsorption kinetics of asphaltenes at the oil-water interface and nanoaggregation in the bulk. *Langmuir* **2012**, *28* (26), 9986−95.
(29) Rane, J. P.; Pauchard, V.; Couzis, A.; Banerjee, S. Interfacial rheology of asphaltenes at oil-water interfaces and interpretation of the equation of state. *Langmuir* **2013**, *29* (15), 4750−9.
(30) Rane, J. P.; Zarkar, S.; Pauchard, V.; Mullins, O. C.; Christie, D.; Andrews, A. B.; Pomerantz, A. E.; Banerjee, S. Applicability of the Langmuir Equation of State for Asphaltene Adsorption at the Oil−Water Interface: Coal-Derived, Petroleum, and Synthetic Asphaltenes. *Energy Fuels* **2015**, *29* (6), 3584−3590.
(31) Klein, G. C.; Kim, S.; Rodgers, R. P.; Marshall, A. G.; Yen, A. Mass Spectral Analysis of Asphaltenes. II. Detailed Compositional Comparison of Asphaltenes Deposit to Its Crude Oil Counterpart for Two Geographically Different Crude Oils by ESI FT-ICR MS. *Energy Fuels* **2006**, *20*, 1973−1979.
(32) Klein, G. C.; Kim, S.; Rodgers, R. P.; Marshall, A. G.; Yen, A.; Asomaning, S. Mass Spectral Analysis of Asphaltenes. I. Compositional Differences between Pressure-Drop and Solvent-Drop Asphaltenes Determined by Electrospray Ionization Fourier Transform Ion Cyclotron Resonance Mass Spectrometry. *Energy Fuels* **2006**, *20*, 1965−1972.
(33) McKenna, A. M.; Donald, L. J.; Fitzsimmons, J. E.; Juyal, P.; Spicer, V.; Standing, K. G.; Marshall, A. G.; Rodgers, R. P. Heavy petroleum composition. 3. Asphaltene aggregation. *Energy Fuels* **2013**, *27* (3), 1246−1256.
(34) Martínez-Haya, B.; Hortal, A. R.; Hurtado, P.; Lobato, M. D.; Pedrosa, J. M. Laser desorption/ionization determination of molecular weight distributions of polyaromatic carbonaceous compounds and their aggregates. *J. Mass Spectrom.* **2007**, *42*, 701−713.
(35) Pinkston, D. S.; Duan, P.; Gallardo, V. A.; Habicht, S. C.; Tan, X.; Qian, K.; Gray, M.; Müllen, K.; Kenttämaa, H. I. Analysis of Asphaltenes and Asphaltene Model Compounds by Laser-Induced Acoustic Desorption/Fourier Transform Ion Cyclotron Resonance Mass Spectrometry. *Energy Fuels* **2009**, *23* (11), 5564−5570.
(36) Borton, D.; Pinkston, D. S.; Hurt, M. R.; Tan, X.; Azyat, K.; Scherer, A.; Tykwinski, R.; Gray, M.; Qian, K.; Kenttämaa, H. I. Molecular Structures of Asphaltenes Based on the Dissociation Reactions of Their Ions in Mass Spectrometry. *Energy Fuels* **2010**, *24*, 5548−5559.
(37) Hurt, M. R.; Borton, D. J.; Choi, H. J.; Kenttämaa, H. I. Comparison of the structures of molecules in coal and petroleum asphaltenes by using mass spectrometry. *Energy Fuels* **2013**, *27* (7), 3653−3658.
(38) Cunico, R. L.; Sheu, E. Y.; Mullins, O. C. Molecular Weight Measurement of UG8 Asphaltene Using APCI Mass Spectrometry. *Pet. Sci. Technol.* **2004**, *22*, 787−798.
(39) Brownlee, D.; Tsou, P.; Aleon, J.; Alexander, C. M.; Araki, T.; Bajt, S.; Baratta, G. A.; Bastien, R.; Bland, P.; Bleuet, P.; et al. Comet 81P/Wild 2 under a microscope. *Science* **2006**, *314* (5806), 1711−6.
(40) Pomerantz, A. E.; Wu, Q.; Mullins, O. C.; Zare, R. N. Laser-Based Mass Spectrometric Assessment of Asphaltene Molecular Weight, Molecular Architecture, and Nanoaggregate Number. *Energy Fuels* **2015**, *29* (5), 2833−2842.
(41) Sabbah, H.; Morrow, A. L.; Pomerantz, A. E.; Zare, R. N. Evidence for Island Structures as the Dominant Architecture of Asphaltenes. *Energy Fuels* **2011**, *25*, 1597−1604.
(42) Sabbah, H.; Pomerantz, A. E.; Wagner, M.; Müllen, K.; Zare, R. N. Laser Desorption Single-Photon Ionization of Asphaltenes: Mass Range, Compound Sensitivity, and Matrix Effects. *Energy Fuels* **2012**, *26* (6), 3521−3526.
(43) Ruiz-Morales, Y. HOMO-LUMO Gap as an Index of Molecular Size and Structure for Polycyclic Aromatic Hydrocarbons (PAHs) and Asphaltenes: A Theoretical Study. I. *J. Phys. Chem. A* **2002**, *106*, 11283−11308.
(44) Ruiz-Morales, Y.; Mullins, O. C. Polycyclic Aromatic Hydrocarbons of Asphaltenes Analyzed by Molecular Orbital Calculations with Optical Spectroscopy. *Energy Fuels* **2007**, *21*, 256−265.

https://dx.doi.org/10.1021/acs.energyfuels.0c00874
Energy Fuels XXXX, XXX, XXX−XXX

(45) Ruiz-Morales, Y.; Mullins, O. C. Measured and simulated electronic absorption and emission spectra of asphaltenes. *Energy Fuels* **2009**, *23* (3), 1169−1177.
(46) Ruiz-Morales, Y.; Wu, X.; Mullins, O. C. Electronic Absorption Edge of Crude Oils and Asphaltenes Analyzed by Molecular Orbital Calculations with Optical Spectroscopy. *Energy Fuels* **2007**, *21*, 944−952.
(47) Schuler, B.; Meyer, G.; Pena, D.; Mullins, O. C.; Gross, L. Unraveling the Molecular Structures of Asphaltenes by Atomic Force Microscopy. *J. Am. Chem. Soc.* **2015**, *137* (31), 9870−6.
(48) Schuler, B.; Fatayer, S.; Meyer, G.; Rogel, E.; Moir, M.; Zhang, Y.; Harper, M. R.; Pomerantz, A. E.; Bake, K. D.; Witt, M.; et al. Heavy Oil Based Mixtures of Different Origins and Treatments Studied by Atomic Force Microscopy. *Energy Fuels* **2017**, *31* (7), 6856−6861.
(49) Wu, Q.; Pomerantz, A. E.; Mullins, O. C.; Zare, R. N. Laser-Based Mass Spectrometric Determination of Aggregation Numbers for Petroleum- and Coal-Derived Asphaltenes. *Energy Fuels* **2014**, *28*, 475−482.
(50) Wang, W.; Taylor, C.; Hu, H.; Humphries, K. L.; Jaini, A.; Kitimet, M.; Scott, T.; Stewart, Z.; Ulep, K. J.; Houck, S.; et al. Nanoaggregates of Diverse Asphaltenes by Mass Spectrometry and Molecular Dynamics. *Energy Fuels* **2017**, *31* (9), 9140−9151.
(51) Betancourt, S. S.; Ventura, G. T.; Pomerantz, A. E.; Viloria, O.; Dubost, F. X.; Zuo, J.; Monson, G.; Bustamante, D.; Purcell, J. M.; Nelson, R. K.; Rodgers, R. P.; Reddy, C. M.; Marshall, A. G.; Mullins, O. C. Nanoaggregates of asphaltenes in a reservoir crude oil and reservoir connectivity. *Energy Fuels* **2009**, *23* (3), 1178−1188.
(52) Mullins, O. C.; Betancourt, S. S.; Cribbs, M. E.; Dubost, F. X.; Creek, J. L.; Andrews, A. B.; Venkataramanan, L. The Collodial Structure of Crude Oil and the Structure of Oil Reservoirs. *Energy Fuels* **2007**, *21*, 2785−2794.
(53) Andreatta, G.; Bostrom, N.; Mullins, O. C. High-Q Ultrasonic Determination of the Critical Nanoaggregate Concentration of Asphaltenes and the Critical Micelle Concentration of Standard Surfactants. *Langmuir* **2005**, *21*, 2728−2736.
(54) Andreatta, G.; Goncalves, C. C.; Buffin, G.; Bostrom, N.; Quintella, C. M.; Arteaga-Larios, F.; Pérez, E.; Mullins, O. C. Nanoaggregates and structure- function relations in asphaltenes. *Energy Fuels* **2005**, *19* (4), 1282−1289.
(55) Zeng, H.; Song, Y.-Q.; Johnson, D. L.; Mullins, O. C. Critical Nanoaggregate Concentration of Asphaltenes by Direct-Current (DC) Eletrical Conductivity. *Energy Fuels* **2009**, *23*, 1201−1208.
(56) Goual, L. Impedance Spectroscopy of Petroleum Fluids at Low Frequency. *Energy Fuels* **2009**, *23*, 2090−2094.
(57) Goual, L.; Sedghi, M.; Zeng, H.; Mostowfi, F.; McFarlane, R.; Mullins, O. C. On the formation and properties of asphaltene nanoaggregates and clusters by DC-conductivity and centrifugation. *Fuel* **2011**, *90* (7), 2480−2490.
(58) Mostowfi, F.; Indo, K.; Mullins, O. C.; McFarlane, R. Asphaltene Nanoaggregates Studied by Centrifugation. *Energy Fuels* **2009**, *23*, 1194−1200.
(59) Indo, K.; Ratulowski, J.; Dindoruk, B.; Gao, J.; Zuo, J.; Mullins, O. C. Asphaltene Nanoaggregates Measured in a Live Crude Oil by Centrifugation. *Energy Fuels* **2009**, *23* (9), 4460−4469.
(60) Wu, Q.; Seifert, D. J.; Pomerantz, A. E.; Mullins, O. C.; Zare, R. N. Constant Asphaltene Molecular and Nanoaggregate Mass in a Gravitationally Segregated Reservoir. *Energy Fuels* **2014**, *28* (5), 3010−3015.
(61) Eyssautier, J.; Espinat, D.; Gummel, J.; Levitz, P.; Becerra, M.; Shaw, J.; Barré, L. Mesoscale Organization in a Physically Separated Vacuum Residue: Comparison to Asphaltenes in a Simple Solvent. *Energy Fuels* **2012**, *26* (5), 2680−2687.
(62) Eyssautier, J.; Hénaut, I.; Levitz, P.; Espinat, D.; Barré, L. Organization of Asphaltenes in a Vacuum Residue: A Small-Angle X-ray Scattering (SAXS)−Viscosity Approach at High Temperatures. *Energy Fuels* **2012**, *26* (5), 2696−2704.
(63) Eyssautier, J.; Levitz, P.; Espinat, D.; Jestin, J.; Gummel, J.; Grillo, I.; Barre, L. Insight into asphaltene nanoaggregate structure inferred by small angle neutron and X-ray scattering. *J. Phys. Chem. B* **2011**, *115* (21), 6827−37.
(64) Mullins, O. C.; Seifert, D. J.; Zuo, J. Y.; Zeybek, M. Clusters of Asphaltene Nanoaggregates Observed in Oilfield Reservoirs. *Energy Fuels* **2013**, *27* (4), 1752−1761.
(65) Chen, L.; Meyer, J.; Campbell, T.; Canas, J.; Betancourt, S. S.; Dumont, H.; Forsythe, J. C.; Mehay, S.; Kimball, S.; Hall, D. L.; Nighswander, J.; Peters, K. E.; Zuo, J. Y.; Mullins, O. C. Applicability of simple asphaltene thermodynamics for asphaltene gradients in oilfield reservoirs: The Flory−Huggins−Zuo Equation of State with the Yen−Mullins model. *Fuel* **2018**, *221*, 216−232.
(66) Hoepfner, M. P.; Fogler, H. S. Multiscale scattering investigations of asphaltene cluster breakup, nanoaggregate dissociation, and molecular ordering. *Langmuir* **2013**, *29* (49), 15423−32.
(67) Maqbool, T.; Raha, S.; Hoepfner, M. P.; Fogler, H. S. Modeling the aggregation of asphaltene nanoaggregates in crude oil-precipitant systems. *Energy Fuels* **2011**, *25* (4), 1585−1596.
(68) Anisimov, M.; Yudin, I.; Nikitin, V.; Nikolaenko, G.; Chernoutsan, A.; Toulhoat, H.; Frot, D.; Briolant, Y. Asphaltene aggregation in hydrocarbon solutions studied by photon correlation spectroscopy. *J. Phys. Chem.* **1995**, *99* (23), 9576−9580.
(69) Yudin, I. K.; Anisimov, M. A. Dynamic light scattering monitoring of asphaltene aggregation in crude oils and hydrocarbon solutions. In *Asphaltenes, Heavy Oils, and Petroleomics*; Mullins, O. C., Sheu, E. Y., Hammami, A., Marshall, A. G., Eds.; Springer: New York, 2007; pp 439−468, DOI: 10.1007/0-387-68903-6_17.
(70) Zuo, J. Y.; Chen, Y.; Pan, S.; Wang, K.; Mullins, O. C. Investigation of density inversion induced by gas charges into oil reservoirs using diffusion equations. *Energy* **2016**, *100*, 199−216.
(71) Zuo, J. Y.; Mullins, O. C.; Jackson, R.; Agarwal, A.; Ayan, C.; Wang, K.; Chen, Y.; Pan, S.; Elshahawi, H.; Dong, C.; Herold, B.; Kumar, S. Understanding Reservoir Fluid Dynamic Processes by Using Diffusive Models. *Proceedings of the Offshore Technology Conference*; Houston, TX, May 2−5, 2016; DOI: 10.4043/26964-MS.
(72) Zuo, J. Y.; Pan, S.; Wang, K.; Mullins, O. C.; Dumont, H.; Chen, L.; Mishra, V.; Canas, J. Analysis of asphaltene instability using diffusive and thermodynamic models during gas charges into oil reservoirs. *Energy Fuels* **2017**, *31* (4), 3717−3728.
(73) Qureshi, A.; Zuo, J. Y.; Seifert, D. J.; Zeybek, M.; Mullins, O. C. Mobile Heavy Oil and Tar Mat Characterization within a Single Oil Column Utilizing Novel Asphaltene Science. *Proceedings of the SPE Kuwait International Petroleum Conference and Exhibition*; Kuwait City, Kuwait, Dec 10−12, 2012; DOI: 10.2118/163291-MS.
(74) Zuo, J. Y.; Jackson, R.; Agarwal, A.; Herold, B.; Kumar, S.; Santo, I. D.; Dumont, H.; Ayan, C.; Beardsell, M.; Mullins, O. C. Diffusion Model Coupled with the Flory−Huggins−Zuo Equation of State and Yen−Mullins Model Accounts for Large Viscosity and Asphaltene Variations in a Reservoir Undergoing Active Biodegradation. *Energy Fuels* **2015**, *29* (3), 1447−1460.
(75) Betancourt, S. S.; Johansen, Y. B.; Forsythe, J. C.; Rinna, J.; Christoffersen, K.; Skillingstad, P.; Achourov, V.; Canas, J.; Chen, L.; Pomerantz, A. E.; Zuo, J. Y.; Mullins, O. C. Gravitational Gradient of Asphaltene Molecules in an Oilfield Reservoir with Light Oil. *Energy Fuels* **2018**, *32* (4), 4911−4924.
(76) Rogel, E.; Ovalles, C.; Bake, K. D.; Zuo, J. Y.; Dumont, H.; Pomerantz, A. E.; Mullins, O. C. Asphaltene Densities and Solubility Parameter Distributions: Impact on Asphaltene Gradients. *Energy Fuels* **2016**, *30* (11), 9132−9140.
(77) Freed, D. E.; Mullins, O. C.; Zuo, J. Y. Heuristics for Equilibrium Distributions of Asphaltenes in the Presence of GOR Gradients. *Energy Fuels* **2014**, *28* (8), 4859−4869.
(78) Mullins, O. C. *The Physics of Reservoir Fluids: Discovery through Downhole Fluid Analysis*; Schlumberger: Houston, TX, 2008.
(79) Johansen, Y. B.; Rinna, J.; Betancourt, S. S.; Forsythe, J. C.; Achourov, V.; Canas, J. A.; Chen, L.; Zuo, J. Y.; Mullins, O. C. Asphaltene Gradient Analysis by DFA Coupled with Geochemical Analysis by GC and GCxGC Indicate Connectivity in Agreement with One Year of Production in a Norwegian Oilfield. *Proceedings of the*

https://dx.doi.org/10.1021/acs.energyfuels.0c00874
Energy Fuels XXXX, XXX, XXX−XXX

SPE Annual Technical Conference and Exhibition; Dallas, TX, Sept, 24−26, 2018; DOI: 10.2118/191490-MS.
(80) Tissot, B.; Welte, D. *Petroleum Formation and Occurrence*, 2nd ed.; Springer: Berlin, Germany, 1984; DOI: 10.1007/978-3-642-87813-8.
(81) Chen, L.; Forsythe, J. C.; Wilkinson, T.; Winkelman, B.; Meyer, J.; Canas, J. A.; Xu, W.; Zuo, J. Y.; Betancourt, S. S.; Shan, D.; Hayden, R. S.; Gendur, J.; Hearn, R.; Kumar, A.; Lake, P.; Mullins, O. C. A Study of Connectivity and Baffles in a Deepwater Gulf of Mexico Reservoir Linking Downhole Fluid Analysis and Geophysics. *Proceedings of the SPE Annual Technical Conference and Exhibition*; San Antonio, Texas, Oct 9−11, 2017; DOI: 10.2118/187231-MS.
(82) Mullins, O. C.; Dumont, H.; Mishra, V. K.; Gomez, A.; Wilkinson, T.; Winkelman, B.; Primio, R. D.; Uchytil, S.; Nagarajan, N.; Strauss, S.; O'Donnell, M.; Seifert, D. J.; Elshahawi, H.; Chen, L.; Pfeiffer, T.; Achourov, V.; Zeybek, M.; Zuo, J. Y.; Forsythe, J.; Betancourt, S. S.; Andrews, A. B.; Pomerantz, A. E. The Critical Role of Asphaltene Gradients and Data Integration in Reservoir Fluid Geodynamics Analysis. *Proceedings of the SPE Annual Technical Conference and Exhibition*; San Antonio, TX, Oct 9−11, 2017; DOI: 10.2118/187277-MS.
(83) Achourov, V.; Pfeiffer, T.; Kollien, T.; Betancourt, S. S.; Zuo, J. Y.; di Primio, R.; Mullins, O. C. Gas diffusion into oil, reservoir baffling and tar mats analyzed by downhole fluid analysis, pressure transients, core extracts and DSTs. *Petrophysics* **2015**, *56* (4), 346−357.
(84) Zuo, J. Y.; Elshahawi, H.; Dong, C.; Latifzai, A. S.; Zhang, D.; Mullins, O. C. DFA Asphaltene Gradients for Assessing Connectivity in Reservoirs under Active Gas Charging. *Proceedings of the SPE Annual Technical Conference and Exhibition*; Denver, CO, Oct 30−Nov 2, 2011; DOI: 10.2118/145438-MS.
(85) Forsythe, J. C.; Martin, R.; De Santo, I.; Tyndall, R.; Arman, K.; Pye, J.; De Nicolais, N.; Nelson, R. K.; Pomerantz, A. E.; Kenyon-Roberts, S.; Zuo, J. Y.; Betancourt, S. S.; Reddy, C.; Peters, K. E.; Mullins, O. C. Integrating comprehensive two-dimensional gas chromatography and downhole fluid analysis to validate a spill-fill sequence of reservoirs with variations of biodegradation, water washing and thermal maturity. *Fuel* **2017**, *191*, 538−554.
(86) Mullins, O. C.; Dumont, H.; Mishra, V.; Pfeiffer, T.; Achourov, V.; Pomerantz, A. E.; Zuo, J. Y.; Tilke, P.; Elshahawi, H.; Di Primio, R. Reservoir evaluation, downhole fluid analysis and reservoir fluid geodynamics. *Proceedings of the SPWLA 57th Annual Logging Symposium*; Reykjavik, Iceland, June 25−29, 2016.
(87) Mullins, O. C.; Primio, R. D.; Zuo, J. Y.; Uchytil, S.; Mishra, V. K.; Dumont, H.; Pfeiffer, T.; Achourov, V. V.; Pomerantz, A. E.; Forsythe, J.; Betancourt, S. S.; Elshahawi, H. Reservoir Fluid Geodynamics; The Link between Petroleum Systems and Production Concerns Relating to Fluids and Tar Distributions in Reservoirs. *Proceedings of the SPE Annual Technical Conference and Exhibition*; Dubai, United Arab Emirates, Sept 26−28, 2016; DOI: 10.2118/181535-MS.
(88) Mullins, O. C.; Fujisawa, G.; Elshahawi, H.; Hashem, M. Coarse and Ultra-Fine Scale Compartmentalization by Downhole Fluid Analysis. *Proceedings of the International Petroleum Technology Conference*; Doha, Qatar, Nov 21−23, 2005; DOI: 10.2523/IPTC-10034-MS.
(89) Mullins, O. C.; Ventura, G. T.; Nelson, R. K.; Betancourt, S. S.; Raghuraman, B.; Reddy, C. M. Visible−near-infrared spectroscopy by downhole fluid analysis coupled with comprehensive two-dimensional gas chromatography to address oil reservoir complexity. *Energy Fuels* **2008**, *22* (1), 496−503.
(90) Dumont, H.; Mullins, O. C.; Zuo, J.; Pomerantz, A. E.; Forsythe, J.; Mishra, V. K.; Garcia, G. Compartments, Connectivity & Baffling Analyzed by the Extent of Equilibration of Asphaltene Gradients Using DFA. *Proceedings of the Offshore Technology Conference*; Houston, TX, May 2−5, 2016; DOI: 10.4043/27143-MS.
(91) Mishra, V. K.; Zuo, J. Y.; Dumont, H.; Mullins, O. C. Permeable tar mat formation described within context of novel asphaltene science. *Proceedings of the SPE Kuwait International Petroleum Conference and Exhibition*; Kuwait City, Kuwait, Dec 10−12, 2012; DOI: 10.2118/163292-MS.
(92) Dumont, H.; Zuo, J. Y.; Mullins, O. C.; Garcia, G.; Mishra, V. K.; Harrison, C.; Fukagawa, S.; Sullivan, M.; Chen, L.; Montesinos, J. Asphaltene and Saturation Pressure Detection with DFA while Pulling out of Hole on Wireline. *Proceedings of the SPWLA 57th Annual Logging Symposium*; Reykjavik, Iceland, June 25−29, 2016.
(93) Chen, Y.; Wang, K.; Chen, L.; Dumont, H.; Mishra, V. K.; Zuo, J. Y.; Mullins, O. C.; Elshahawi, H. Variation of Asphaltene Onset Pressure Due to Reservoir Fluid Disequilibrium. *Proceedings of the Offshore Technology Conference*; Houston, TX, May 5−8, 2014; DOI: 10.4043/25172-MS.
(94) Uchytil, S.; Mishra, V. K.; Betancourt, S. S.; Guthrie, J.; Huang, J.; Teerman, S.; Nguyen, A.; Evans, S.; Nagarajan, N.; Mullins, O. C. Impact of a Secondary Condensate Charge into an Oil Reservoir Evaluated by Downhole Fluid Analysis, Core Analysis, and Production. *Proceedings of the Offshore Technology Conference*; Houston, TX, May 2−5, 2016; DOI: 10.4043/27240-MS.
(95) Dong, C.; Hows, M. P.; Cornelisse, P. M.; Elshahawi, H. Fault Block Migrations Inferred from Asphaltene Gradients. *Proceedings of the SPWLA 54th Annual Logging Symposium*; New Orleans, LA, June 22−26, 2013.
(96) Chen, L.; Winkelman, B.; Wilkinson, T.; Meyer, J.; Mullins, O. C.; Forsythe, J. C.; Hayden, R. S.; Xu, W.; Shan, D.; Canas, J. A.; Garcia, G.; Zuo, J. Y.; Gan, Y.; Chao, J. C.; Hall, D. L. Using Formation Testing and Asphaltene Gradient Modeling to Guide G&G Modeling and Field Development—A Fault Block Migration Study. *Proceedings of the SPE Annual Technical Conference and Exhibition*; Dallas, TX, Sept 24−26, 2018; DOI: 10.2118/191499-MS.
(97) Forsythe, J. C.; De Santo, I.; Martin, R.; Tyndall, R.; Arman, K.; Pye, J.; O'Donnell, M.; Kenyon-Roberts, S.; Nelson, R. K.; Reddy, C. M.; Pomerantz, A. E.; Canas, J. A.; Zuo, J. Y.; Peters, K. E.; Mullins, O. C. Reservoir implications of a spill-fill sequence of reservoir charge coupled with viscosity and asphaltene gradients from a combination of water washing and biodegradation. *Proceedings of the SPE Annual Technical Conference and Exhibition*; San Antonio, TX, Oct 9−11, 2017; DOI: 10.2118/187044-MS.
(98) Mullins, O. C.; Johansen, Y. B.; Rinna, J.; Meyer, J.; Kenyon-Roberts, S.; Chen, L.; Forsythe, J. C.; Achourov, V.; Jackson, R.; Betancourt, S. S. Diverse Fluid Gradients Associated with Biodegradation of Crude Oil. *Proceedings of the SPWLA 60th Annual Logging Symposium*; The Woodlands, TX, June 15−19, 2019.
(99) Forsythe, J. C.; Kenyon-Roberts, S.; O'Donnell, M.; Betancourt, S. S.; Masurek, N.; Gisolf, A.; Bennett, B.; Nelson, R. K.; Canas, J. A.; Reddy, C. M.; Peters, K. E.; Zuo, J. Y.; Mullins, O. C. Biodegradation and water washing in a spill-fill sequence of oilfields. *Fuel* **2019**, *237*, 707−719.
(100) Bertolini, A. C.; Monteiro, J.; Canas, J. A.; Betancourt, S. S.; Mullins, O. C.; Colacelli, S.; Polinski, R. K. Reservoir Fluid Geodynamics in Brazilian Presalt Carbonate Field. *Proceedings of the SPE Middle East Oil and Gas Show and Conference*; Manama, Bahrain, March 18−21, 2019; DOI: 10.2118/194841-MS.
(101) Chen, L.; Gan, Y.; Gao, B.; Chen, J.; Canas, J. A.; Jackson, R.; EI-Khoury, J.; Mullins, O. C. Reservoir Fluid Geodynamics, a New Way to Evaluate the Reservoir Connectivity and Crude Oil Alteration with Late Gas Charge. *Proceedings of the International Petroleum Technology Conference*; Beijing, China, March 26−28, 2019; DOI: 10.2523/IPTC-19472-MS.
(102) Datir, H. B.; Cavalleri, C.; Kollien, T.; Achourov, V.; Mullins, O. C. Realization of Reservoir of Fluid Geodynamics with the Integration of Petrophysics and Downhole Fluid Analysis. *Proceedings of the SPWLA 59th Annual Logging Symposium*; London, U.K., June 2−6, 2018.
(103) Mullins, O. C.; Primio, R. D.; Uchytil, S.; Zuo, J. Y.; Dumont, H.; Mishra, V.; Pfeiffer, T.; Achourov, V. Bitumen and Tar Deposition and Tar Mat Formation Accounted for by Multiple Charging, Trap Filling and Fluid Geodynamics. *Proceedings of the SPE Annual Technical Conference and Exhibition*; Dubai, United Arab Emirates, Sept 26−28, 2016; DOI: 10.2118/181544-MS.

https://dx.doi.org/10.1021/acs.energyfuels.0c00874
Energy Fuels XXXX, XXX, XXX−XXX

(104) Mullins, O. C.; Zuo, J. Y.; Pomerantz, A. E.; Forsythe, J. C.; Peters, K. Reservoir Fluid Geodynamics: The Chemistry and Physics of Oilfield Reservoir Fluids after Trap Filling. *Energy Fuels* **2017**, *31* (12), 13088−13119.
(105) Wang, K.; Kauerauf, A. I.; Zuo, J. Y.; Chen, Y.; Dong, C.; Elshahawi, H.; Mullins, O. C. Differing Equilibration Times of GOR, Asphaltenes and Biomarkers as Determined by Charge History and Reservoir Fluid Geodynamics. *Petrophysics* **2015**, *56* (5), 440−456.
(106) Andrews, A. B.; McClelland, A.; Korkeila, O.; Demidov, A.; Krummel, A.; Mullins, O. C.; Chen, Z. Molecular orientation of asphaltenes and PAH model compounds in Langmuir- Blodgett films using sum frequency generation spectroscopy. *Langmuir* **2011**, *27* (10), 6049−6058.
(107) Redelius, P. G. Solubility parameters and bitumen. *Fuel* **2000**, *79*, 27−35.
(108) Ruiz-Morales, Y.; Mullins, O. C. Coarse-grained molecular simulations to investigate asphaltenes at the oil−water interface. *Energy Fuels* **2015**, *29* (3), 1597−1609.
(109) Liu, F. Understanding Asphaltenes Adsorption at Liquid-Liquid and Liquid-Solid Interfaces. Ph.D. Thesis, City College of New York, New York, 2020.
(110) Sztukowski, D. M.; Yarranton, H. W. Rheology of asphaltene-toluene/water interfaces. *Langmuir* **2005**, *21* (25), 11651−11658.
(111) Freer, E.; Radke, C. Relaxation of asphaltenes at the toluene/water interface: Diffusion exchange and surface rearrangement. *J. Adhes.* **2004**, *80* (6), 481−496.
(112) Daniel, R. C.; Berg, J. C. A simplified method for predicting the dynamic surface tension of concentrated surfactant solutions. *J. Colloid Interface Sci.* **2003**, *260* (1), 244−249.
(113) Menger, F. M.; Rizvi, S. A. Relationship between surface tension and surface coverage. *Langmuir* **2011**, *27* (23), 13975−13977.
(114) Yang, F.; Tchoukov, P.; Dettman, H.; Teklebrhan, R. B.; Liu, L.; Dabros, T.; Czarnecki, J.; Masliyah, J.; Xu, Z. Asphaltene subfractions responsible for stabilizing water-in-crude oil emulsions. Part 2: Molecular representations and molecular dynamics simulations. *Energy Fuels* **2015**, *29* (8), 4783−4794.
(115) Strausz, O. P.; Mojelsky, T. W.; Lown, E. M. The molecular structure of asphaltene: An unfolding story. *Fuel* **1992**, *71* (12), 1355−1363.
(116) Boduszynski, M. M., Asphaltenes in Petroleum Asphalts. In *Chemistry of Asphaltenes*; Bunger, J. W., Li, N. C., Eds.; American Chemical Society (ACS): Washington, D.C., 1982; Advances in Chemistry, Vol. *195*, Chapter 7, pp 119−135, DOI: 10.1021/ba-1981-0195.ch007.
(117) Herod, A. A.; Bartle, K. D.; Kandiyoti, R. Characterization of Heavy Hydrocarbons by Chromatographic and Mass Spectrometric Methods: An Overview. *Energy Fuels* **2007**, *21*, 2176−2203.
(118) Gray, M. R. Consistency of asphaltene chemical structures with pyrolysis and coking behavior. *Energy Fuels* **2003**, *17* (6), 1566−1569.
(119) Alshareef, A. H.; Scherer, A.; Tan, X.; Azyat, K.; Stryker, J. M.; Tykwinski, R. R.; Gray, M. R. Formation of Archipelago Structures during Thermal Cracking Implicates a Chemical Mechanism for the Formation of Petroleum Asphaltenes. *Energy Fuels* **2011**, *25* (5), 2130−2136.
(120) Groenzin, H.; Mullins, O. C. Molecular size and structure of asphaltenes. *Pet. Sci. Technol.* **2001**, *19* (1−2), 219−230.
(121) Calemma, V.; Iwanski, P.; Nali, M.; Scotti, R.; Montanari, L. Structural Characterization of Asphaltenes of Different Origins. *Energy Fuels* **1995**, *9* (2), 225−230.
(122) Scotti, R.; Montanari, L. Molecular structure and intermolecular interaction of asphaltenes by FT-IR, NMR, EPR. In *Structures and Dynamics of Asphaltenes*; Mullins, O. C., Sheu, E. Y., Eds.; Springer: Boston, MA, 1998; pp 79−113, DOI: 10.1007/978-1-4899-1615-0_3.
(123) Ruiz-Morales, Y.; Mullins, O. C. Singlet−Triplet and Triplet−Triplet Transitions of Asphaltene PAHs by Molecular Orbital Calculations. *Energy Fuels* **2013**, *27* (9), 5017−5028.
(124) Ralston, C. Y.; Wu, X.; Mullins, O. C. Quantum yields of crude oils. *Appl. Spectrosc.* **1996**, *50* (12), 1563−1568.
(125) Sabbah, H.; Morrow, A. L.; Pomerantz, A. E.; Mullins, O. C.; Tan, X.; Gray, M. R.; Azyat, K.; Tykwinski, R. R.; Zare, R. N. Comparing Laser Desorption/Laser Ionization Mass Spectra of Asphaltenes and Model Compounds. *Energy Fuels* **2010**, *24*, 3589−3594.
(126) Wu, Q.; Pomerantz, A. E.; Mullins, O. C.; Zare, R. N. Minimization of Fragmentation and Aggregation by Laser Desorption Laser Ionization Mass Spectrometry. *J. Am. Soc. Mass Spectrom.* **2013**, *24*, 1116−1122.
(127) Zare, R. N.; Hahn, J. H.; Zenobi, R. Mass Spectrometry of Molecular Adsorbates Using Laser Desorption/Laser Multiphoton Ionization. *Bull. Chem. Soc. Jpn.* **1988**, *61*, 87−92.
(128) Maechling, C. R.; Clemett, S. J.; Engelke, F.; Zare, R. N. Evidence for thermalization of surface-desorbed molecules at heating rates of 10^8 K/s. *J. Chem. Phys.* **1996**, *104*, 8768−8776.
(129) Hunt, J.-E.; Winans, R.-E.; Miller, J. Characterization of Asphaltenes from Processed Resids; *Proceedings of the 213th ACS National Meeting*; San Francisco, CA, April 13−17, 1997.
(130) Al-Muhareb, E.; Morgan, T. J.; Herod, A. A.; Kandiyoti, R. Characterization of Petroleum Asphaltenes by Size Exclusion Chromatography, UV-fluorescence and Mass Spectrometry. *Pet. Sci. Technol.* **2007**, *25*, 81−91.
(131) Hurtado, P.; Hortal, A. R.; Martínez-Haya, B. Matrix-assisted laser desorption/ionization detection of carbonaceous compounds in ionic liquid matrices. *Rapid Commun. Mass Spectrom.* **2007**, *21*, 3161−3164.
(132) Sugihara, G.; Hisatomi, M. Enthalpy−entropy compensation phenomenon observed for different surfactants in aqueous solution. *J. Colloid Interface Sci.* **1999**, *219* (1), 31−36.
(133) Burya, Y. G.; Yudin, I. K.; Dechabo, V. A.; Kosov, V. I.; Anisimov, M. A. Light-scattering study of petroleum asphaltene aggregation. *Appl. Opt.* **2001**, *40* (24), 4028−4035.
(134) Goual, L.; Sedghi, M.; Mostowfi, F.; McFarlane, R.; Pomerantz, A. E.; Saraji, S.; Mullins, O. C. Cluster of Asphaltene Nanoaggregates by DC Conductivity and Centrifugation. *Energy Fuels* **2014**, *28* (8), 5002−5013.
(135) Gross, L.; Mohn, F.; Moll, N.; Liljeroth, P.; Meyer, G. The chemical structure of a molecule resolved by atomic force microscopy. *Science* **2009**, *325* (5944), 1110−1114.
(136) Moll, N.; Gross, L.; Mohn, F.; Curioni, A.; Meyer, G. The mechanisms underlying the enhanced resolution of atomic force microscopy with functionalized tips. *New J. Phys.* **2010**, *12* (12), 125020.
(137) Mohn, F.; Schuler, B.; Gross, L.; Meyer, G. Different tips for high-resolution atomic force microscopy and scanning tunneling microscopy of single molecules. *Appl. Phys. Lett.* **2013**, *102* (7), 073109.
(138) Pavliček, N.; Mistry, A.; Majzik, Z.; Moll, N.; Meyer, G.; Fox, D. J.; Gross, L. Synthesis and characterization of triangulene. *Nat. Nanotechnol.* **2017**, *12* (4), 308−311.
(139) Majzik, Z.; Pavliček, N.; Vilas-Varela, M.; Pérez, D.; Moll, N.; Guitián, E.; Meyer, G.; Peña, D.; Gross, L. Studying an antiaromatic polycyclic hydrocarbon adsorbed on different surfaces. *Nat. Commun.* **2018**, *9* (1), 1198.
(140) Schuler, B.; Liu, W.; Tkatchenko, A.; Moll, N.; Meyer, G.; Mistry, A.; Fox, D.; Gross, L. Adsorption Geometry Determination of Single Molecules by Atomic Force Microscopy. *Phys. Rev. Lett.* **2013**, *111* (10), 106103.
(141) Pavliček, N.; Fleury, B.; Neu, M.; Niedenführ, J.; Herranz-Lancho, C.; Ruben, M.; Repp, J. Atomic Force Microscopy Reveals Bistable Configurations of Dibenzo[a, h]thianthrene and their Interconversion Pathway. *Phys. Rev. Lett.* **2012**, *108* (8), 086101.
(142) Schuler, B.; Zhang, Y.; Collazos, S.; Fatayer, S.; Meyer, G.; Pérez, D.; Guitián, E.; Harper, M. R.; Kushnerick, J. D.; Pena, D.; Gross, L. Characterizing aliphatic moieties in hydrocarbons with atomic force microscopy. *Chem. Sci.* **2017**, *8* (3), 2315−2320.

https://dx.doi.org/10.1021/acs.energyfuels.0c00874
Energy Fuels XXXX, XXX, XXX−XXX

(143) Moll, N.; Schuler, B.; Kawai, S.; Xu, F.; Peng, L.; Orita, A.; Otera, J.; Curioni, A.; Neu, M.; Repp, J.; Meyer, G.; Gross, L. Image Distortions of a Partially Fluorinated Hydrocarbon Molecule in Atomic Force Microscopy with Carbon Monoxide Terminated Tips. *Nano Lett.* **2014**, *14* (11), 6127−6131.
(144) Zahl, P.; Zhang, Y. Guide for Atomic Force Microscopy Image Analysis To Discriminate Heteroatoms in Aromatic Molecules. *Energy Fuels* **2019**, *33* (6), 4775−4780.
(145) Mohn, F.; Gross, L.; Moll, N.; Meyer, G. Imaging the charge distribution within a single molecule. *Nat. Nanotechnol.* **2012**, *7* (4), 227−231.
(146) Giessibl, F. J. High-speed force sensor for force microscopy and profilometry utilizing a quartz tuning fork. *Appl. Phys. Lett.* **1998**, *73* (26), 3956−3958.
(147) Repp, J.; Meyer, G.; Stojković, S. M.; Gourdon, A.; Joachim, C. Molecules on Insulating Films: Scanning-Tunneling Microscopy Imaging of Individual Molecular Orbitals. *Phys. Rev. Lett.* **2005**, *94* (2), 026803.
(148) Gross, L.; Schuler, B.; Pavliček, N.; Fatayer, S.; Majzik, Z.; Moll, N.; Peña, D.; Meyer, G. Atomic Force Microscopy for Molecular Structure Elucidation. *Angew. Chem., Int. Ed.* **2018**, *57* (15), 3888−3908.
(149) Gross, L.; Mohn, F.; Moll, N.; Meyer, G.; Ebel, R.; Abdel-Mageed, W. M.; Jaspars, M. Organic structure determination using atomic-resolution scanning probe microscopy. *Nat. Chem.* **2010**, *2* (10), 821−825.
(150) de Oteyza, D. G.; Gorman, P.; Chen, Y.-C.; Wickenburg, S.; Riss, A.; Mowbray, D. J.; Etkin, G.; Pedramrazi, Z.; Tsai, H.-Z.; Rubio, A.; Crommie, M. F.; Fischer, F. R. Direct Imaging of Covalent Bond Structure in Single-Molecule Chemical Reactions. *Science* **2013**, *340* (6139), 1434−1437.
(151) Schuler, B.; Fatayer, S.; Mohn, F.; Moll, N.; Pavliček, N.; Meyer, G.; Peña, D.; Gross, L. Reversible Bergman cyclization by atomic manipulation. *Nat. Chem.* **2016**, *8* (3), 220−224.
(152) Fatayer, S.; Poddar, N. B.; Quiroga, S.; Schulz, F.; Schuler, B.; Kalpathy, S. V.; Meyer, G.; Pérez, D.; Guitián, E.; Peña, D.; Wornat, M. J.; Gross, L. Atomic Force Microscopy Identifying Fuel Pyrolysis Products and Directing the Synthesis of Analytical Standards. *J. Am. Chem. Soc.* **2018**, *140* (26), 8156−8161.
(153) Chen, P.; Metz, J. N.; Mennito, A. S.; Merchant, S.; Smith, S. E.; Siskin, M.; Rucker, S. P.; Dankworth, D. C.; Kushnerick, J. D.; Yao, N.; Zhang, Y. Petroleum pitch: Exploring a 50-year structure puzzle with real-space molecular imaging. *Carbon* **2020**, *161*, 456−465.
(154) Zhang, Y.; Schuler, B.; Fatayer, S.; Gross, L.; Harper, M. R.; Kushnerick, J. D. Understanding the Effects of Sample Preparation on the Chemical Structures of Petroleum Imaged with Noncontact Atomic Force Microscopy. *Ind. Eng. Chem. Res.* **2018**, *57* (46), 15935−15941.
(155) Beuhler, R.; Flanigan, E.; Greene, L.; Friedman, L. Proton transfer mass spectrometry of peptides. Rapid heating technique for underivatized peptides containing arginine. *J. Am. Chem. Soc.* **1974**, *96* (12), 3990−3999.
(156) Chacón-Patiño, M. L.; Rowland, S. M.; Rodgers, R. P. Advances in Asphaltene Petroleomics. Part 3. Dominance of island or archipelago structural motif is sample dependent. *Energy Fuels* **2018**, *32* (9), 9106−9120.
(157) Chacón-Patiño, M. L.; Rowland, S. M.; Rodgers, R. P. Advances in asphaltene petroleomics. Part 2: Selective separation method that reveals fractions enriched in island and archipelago structural motifs by mass spectrometry. *Energy Fuels* **2018**, *32* (1), 314−328.
(158) Chacón-Patiño, M. L.; Rowland, S. M.; Rodgers, R. P. Advances in asphaltene petroleomics. Part 1: Asphaltenes are composed of abundant island and archipelago structural motifs. *Energy Fuels* **2017**, *31* (12), 13509−13518.
(159) Hughey, C. A.; Rodgers, R. P.; Marshall, A. G. Resolution of 11 000 compositionally distinct components in a single electrospray ionization Fourier transform ion cyclotron resonance mass spectrum of crude oil. *Anal. Chem.* **2002**, *74* (16), 4145−4149.
(160) Kew, W.; Blackburn, J. W.; Uhrín, D. a. Response to comment on "laser desorption/ionization coupled to FTICR mass spectrometry for studies of natural organic matter. *Anal. Chem.* **2018**, *90* (9), 5968−5971.
(161) Hansen, C. M. *Hansen Solubility Parameters: A User's Handbook*; CRC Press: Boca Raton, FL, 2002.
(162) George, G. N.; Gorbaty, M. L. Sulfur K-Edge X-ray Absorption Spectroscopy of Petroleum Asphaltenes and Model Compounds. *J. Am. Chem. Soc.* **1989**, *111*, 3182−3186.
(163) Mitra-Kirtley, S.; Mullins, O. C. Sulfur chemical moieties in carbonaceous materials. In *Asphaltenes, Heavy Oils, and Petroleomics*; Mullins, O. C., Sheu, E. Y., Hammami, A., Marshall, A. G., Eds.; Springer: New York, 2007; pp 157−188, DOI: 10.1007/0-387-68903-6_6.
(164) Mitra-Kirtley, S.; Mullins, O. C.; van Elp, J.; George, S. J.; Chen, J.; Cramer, S. P. Determination of the Nitrogen Chemical Structures in Petroleum Asphaltenes Using XANES Spectroscopy. *J. Am. Chem. Soc.* **1993**, *115*, 252−258.
(165) Moschopedis, S. E.; Speight, J. G. Oxygen functions in asphaltenes. *Fuel* **1976**, *55* (4), 334−336.
(166) Lin, M. S.; Lunsford, K. M.; Glover, C. J.; Davison, R. R.; Bullin, J. A. The Effects of Asphaltenes on the Chemical and Physical Characteristics of Asphalt. In *Asphaltenes: Fundamentals and Applications*; Sheu, E. Y., Mullins, O. C., Eds.; Springer: Boston, MA, 1995; pp 155−176, DOI: 10.1007/978-1-4757-9293-5_5.
(167) Lin, M.-S.; Chaffin, J.; Davison, R.; Glover, C.; Bullin, J. A new suspension viscosity model and its application to asphaltene association thermodynamics and structures. In *Structures and Dynamics of Asphaltenes*; Mullins, O. C., Sheu, E. Y., Eds.; Springer: Boston, MA: 1998; pp 267−302, DOI: 10.1007/978-1-4899-1615-0_9.
(168) Pal, R.; Rhodes, E. Viscosity/concentration relationships for emulsions. *J. Rheol.* **1989**, *33* (7), 1021−1045.
(169) Baltus, R. E. Characterization of asphaltenes and heavy oils using hydrodynamic property measurements. In *Structures and Dynamics of Asphaltenes*; Mullins, O. C., Sheu, E. Y., Eds.; Springer: Boston, MA, 1998; pp 303−335, DOI: 10.1007/978-1-4899-1615-0_10.
(170) Storm, D. A.; Barresi, R. J.; Sheu, E. Y. Solvation of Ratawi Asphaltenes in Vacuum Residue. In *Asphaltene Particles in Fossil Fuel Exploration, Recovery, Refining, and Production Processes*; Sharma, M. K., Yen, T. F., Eds.; Springer: Boston, MA, 1994; pp 185−191, DOI: 10.1007/978-1-4615-2456-4_15.
(171) Pierre, A. C. *Introduction to Sol-Gel Processing*; Springer: New York: 1998; Vol. *1*, DOI: 10.1007/978-1-4615-5659-6.
(172) https://www.promega.com/resources/pubhub/enotes/what-percentage-agarose-is-needed-to-sufficiently-resolve-my-dna-sample/.
(173) Karcher, S. J. *Molecular Biology: A Project Approach*; Academic Press: San Diego, CA, 1995.
(174) Horkay, F.; Douglas, J. F. Polymer Gels: Basics, Challenges, and Perspectives. In *Gels and Other Soft Amorphous Solids*; Horkay, F., Douglas, J. F., Del Gado, E., Eds.; American Chemical Society (ACS): Washington, D.C., 2018; ACS Symposium Series, Vol. *1296*, Chapter 1, pp 1−13, DOI: 10.1021/bk-2018-1296.ch001.
(175) Douglas, J. F. Weak and strong gels and the emergence of the amorphous solid state. *Gels* **2018**, *4* (1), 19.

https://dx.doi.org/10.1021/acs.energyfuels.0c00874
Energy Fuels XXXX, XXX, XXX−XXX